

Article

Pressure Behavior in a Linear Porous Media for Partially Miscible Displacement of Oil by Gas

Luara K. S. Sousa , Wagner Q. Barros , Adolfo P. Pires  and Alvaro M. M. Peres 

Laboratório de Engenharia e Exploração de Petróleo, Universidade Estadual do Norte Fluminense Darcy Ribeiro, Rodovia Amaral Peixoto, Km 163, Imboassica, Macaé 27925-310, Brazil; luara_kss@hotmail.com (L.K.S.S.); adolfo.puime@gmail.com (A.P.P.); alvaroperes@lenep.uenf.br (A.M.M.P.)

* Correspondence: wagnerqb@gmail.com; Tel.: +44-7539-431287

Abstract: Miscible gas flooding improves oil displacement through mass exchange between oil and gas phases. It is one of the most efficient enhanced oil recovery methods for intermediate density oil reservoirs. In this work, analytical solutions for saturation, concentration and pressure are derived for oil displacement by a partially miscible gas injection at a constant rate. The mathematical model considers two-phase, three-component fluid flow in a one-dimensional homogeneous reservoir initially saturated by a single oil phase. Phase saturations and component concentrations are described by a 2×2 hyperbolic system of partial differential equations, which is solved by the method of characteristics. Once this Goursat–Riemann problem is solved, the pressure drop between two points in the porous media is obtained by the integration of Darcy’s law. The solution of this problem may present three different fluid regions depending on the rock–fluid parameters: a single-phase gas region near the injection point, followed by a two-phase region where mass transfer takes place and a single-phase oil region. We considered the single-phase gas and the two-phase gas/oil regions as incompressible, while the single-phase oil region may be incompressible or slightly compressible. The solutions derived in this work are applied for a specific set of rock and fluid properties. For this data set, the two-phase region displays rarefaction waves, shock waves and constant states. The pressure behavior depends on the physical model (incompressible, compressible and finite or infinite porous media). In all cases, the injection pressure is the result of the sum of two terms: one represents the effect of the mobility contrast between phases and the other represents the single-phase oil solution. The solutions obtained in this work are compared to an equivalent immiscible solution, which shows that the miscible displacement is more efficient.

Keywords: enhanced oil recovery; miscible methods; gas flooding; wellbore pressure; injectivity test



Academic Editors: Jun Yao, Priscilla Ribeiro Vargas and Faik Hamad

Received: 29 November 2024

Revised: 13 January 2025

Accepted: 17 January 2025

Published: 21 January 2025

Citation: Sousa, L.K.S.; Barros, W.Q.; Pires, A.P.; Peres, A.M.M. Pressure Behavior in a Linear Porous Media for Partially Miscible Displacement of Oil by Gas. *Fluids* **2025**, *10*, 21. <https://doi.org/10.3390/fluids10020021>

Copyright: © 2025 by the authors. Licensee MDPI, Basel, Switzerland. This article is an open access article distributed under the terms and conditions of the Creative Commons Attribution (CC BY) license (<https://creativecommons.org/licenses/by/4.0/>).

1. Introduction

The main objective of enhanced oil recovery (EOR) is the increase in hydrocarbon recovery by the injection of fluids and/or materials not initially present in the porous media [1]. EOR processes may be classified according to their main physical–chemical drive mechanism: thermal, chemical or miscible [1]. Gas flooding is the second most used secondary recovery technique [2], which has been applied to the field as early as 1917 [3]. The first field applications were pressure maintenance only, but around 1950, projects of oil displacement by miscible gas flooding appeared.

Mathematical models that consider mass transfer between phases have been presented in the literature since the 1960s. Some of these models may be used to predict oil displace-

ment efficiency by miscible gas injection. The fluid flow in porous media with mass transfer can be represented by a system of first-order hyperbolic partial differential equations if second-order effects (such as capillary pressure, gravity and dispersion) are neglected. These equations represent the overall mass conservation of each component [4].

The estimation of the minimum solvent volume required to completely recover the reservoir oil volume was presented in Johnson and Welge [5] and Welge et al. [6]. These authors considered oil displaced by solvent injection in a one-dimensional homogeneous reservoir initially saturated by oil. Based on the Buckley–Leverett frontal-advance theory [7], Wachmann [8] presented a solution for oil displacement by solvent injection for a three-component system (oil/water/alcohol). The mathematical model was also one-dimensional, dispersion and capillary pressure were neglected and the vapor–liquid phase equilibria were modeled using geometric thermodynamic variables. The 2×2 hyperbolic system was solved by the method of characteristics (MOC). Posteriorly, Larson [9], Hirasaki [10], Hirasaki [11] and Dumore et al. [12] extended the work of Wachmann [8] for different types of fluids and reservoir boundary conditions.

Helfferich [13] generalized the theory of displacement in porous media with mass transfer for multicomponent multiphase systems. In his work, the developed theory was applied for ternary systems only.

The first solutions for quaternary systems were reported by Monroe et al. [14]. The cross tie-line concept, introduced in their work, was used to build a unique solution path connecting the initial and the boundary conditions. However, only solutions composed of shocks were presented. Detailed investigations of four-component system behavior with and without change in the volume of mixing were presented later [15–17].

Johns and Orr Jr. [18] analyzed the application of the two-phase displacement theory of oil by gas with mass transfer to a system with n -components. The solutions were obtained by the method of characteristics, and the thermodynamic equilibrium was represented from a series of quaternary diagrams. Next, several approaches for the construction of analytical solutions for n -component systems were presented [19,20].

Three-phase flow may appear in different enhanced oil recovery processes. LaForce and Johns [21] modeled a partially miscible one-dimensional three-phase three-component flow. The solutions were obtained for different initial and injection conditions and were compared to the results of a finite-difference numerical simulator. Barros et al. [22] extended the one-dimensional three-phase solutions for concave relative permeability curves, showing how these relative permeability curves affect the characteristic propagation in the hyperbolic system.

Enhanced oil recovery project management heavily depends on reliable reservoir data. A valuable source of dynamic information comes from well tests. A pressure transient analysis (PTA) provides estimates for several reservoir and well properties, such as the permeability, reservoir average pressure, presence of flow barriers, near-wellbore formation damage and productivity and injectivity indexes. Parameter estimation from a PTA requires analytical or numerical solutions that model the physical phenomena taking place at the wellbore–reservoir interface and at the porous media far away from the well.

There are several analytical models in the literature that describe the pressure behavior during water injection into oil reservoirs. Abbaszadeh and Kamal [23] presented analytical solutions for both injectivity and falloff tests for vertical wells in an oil reservoir under waterflooding. Their solutions were obtained by superimposing pressure-transient effects on a water saturation profile calculated beforehand by the Buckley–Leverett frontal-advance equations. Bratvold and Horne [24] also relied on the Buckley–Leverett theory to obtain an analytical solution for water injectivity tests in oil reservoirs by means of the Boltzmann

self-similar transform. They also derived a falloff semi-analytical solution by discretization of the spatial domain into several concentric rings.

Thompson and Reynolds [25] presented a theory for multiphase flow in radially heterogeneous reservoirs. They observed that, for typical reservoir and fluid properties, the saturation front is always within a steady-state-like region that continuously propagates into the reservoir during the injection period. If the saturation profile is known, a pressure solution can be obtained by the integration of the multiphase Darcy's law over the radial coordinate. Several papers were published based on their hindsight to solve more complex problems. Peres and Reynolds [26] presented an analytical solution for the wellbore pressure behavior during water injectivity tests for both horizontal and vertical wells. Their solution also models water injection into damaged reservoirs that results in a very distinct wellbore pressure behavior. Boughrara et al. [27] extended the injectivity solution of Peres and Reynolds to restricted-entry vertical wells and to horizontal wells in anisotropic reservoirs.

Miscible gas flooding, and other EOR methods as well, lead to more complex mathematical models. There is a lack of published articles that address the wellbore pressure behavior for multicomponent, multiphase flow in porous media.

Habte et al. [28] derived a semi-analytical pressure solution for injectivity and falloff tests for immiscible gas injection following water injection in an oil reservoir. Their procedure first solves the hyperbolic equations for saturation numerically assuming the gas phase as incompressible. Then, the pressure solution is calculated solving a matrix problem formed by the spatial discretization. Machado et al. [29] presented analytical solutions for the two-phase radial flow of oil displacement by carbonated water injection. Concentration and saturation profiles were found using the method of characteristics.

An analytical solution for the pressure behavior during miscible gas injection in an oil reservoir for constant wellbore pressure injection was presented by Mu et al. [30]. In their paper, the effects of miscibility on the relative permeability curves and phase viscosities were modeled by correlations. The saturation profile was obtained by applying the Buckley–Leverett theory, and once this profile was determined, Darcy's law was integrated to calculate the pressure profile.

Cantagesso et al. [31] presented results for the saturation, component concentrations and pressure behavior of a two-phase multicomponent incompressible system, which models miscible gas injection into a one-dimensional homogeneous oil reservoir. The vapor–liquid phase equilibria were modeled using geometric thermodynamic variables. The phase saturation and component concentrations were solved by the MOC, and the pressure solution was obtained by the integration of Darcy's law. Their solution considers that the fluids are incompressible in both single- and two-phase regions. The validity of Darcy's law in homogeneous one-dimensional flow was discussed in Nichele and Teixeira [32], showing that this hypothesis is valid in regions with low inertial effects, i.e., low-velocity, typical for low or slightly low compressibility fluid flow in porous media.

There are different experimental techniques applied to describe miscible multiphase flow in porous media. Core-flooding experiments are performed through the controlled displacement of oil in linear rock plugs, both in immiscible and miscible conditions, and the results can be matched with numerical and analytical results (Hustad and Holt [33]). So, it is possible to investigate the influence of miscible injection in the oil viscosity and its impact in the recovery factor (Dyer and Farouq Ali [34]) and the impact of rock–fluid interaction parameters on oil displacement [35–37]. Another very useful experimental technique is the injection in micro-models, where rock plugs are replaced by synthetic porous media with controlled geometry (Zhang et al. [38], Yang et al. [39], Zou et al. [40]). The results of these experiments can be validated by different numerical experiments (Irannezhad et al. [41,42], Li et al. [43]).

Another very useful technique to understand multiphase flows is numerical reservoir simulation. By using compositional models, it is possible to have an accurate description of thermodynamic and hydrodynamic effects, combined with a complex geological and geometrical reservoir description (Christensen et al. [44]). Numerical simulation is also useful to analyze the mass transfer effects between the injected fluid and the oil in place and its impact on the oil recovery factor (Li et al. [45], Chen et al. [46], Ren et al. [47], Zhu et al. [48]). This effect is specially important for CO₂ injection in low-temperature reservoirs, which leads to complex thermodynamic effects.

In this paper, we extend the solution of Cantagesso et al. [31] to a mixed incompressible–slightly compressible fluid system. The saturation solution shows that, after the gas injection starts, three different fluid regions may appear: a single-phase gas region near the injection (inlet) point, followed by a two-phase gas/oil region where mass transfer takes place and a single-phase oil zone that extends to the porous media outlet as in Figure 1). The first two regions are considered incompressible, while the oil region is taken as slightly compressible. Darcy’s law integration over the spatial domain is used to find the pressure profile. This paper improves the current state of the art in the following topics:

- The application of the Thompson and Reynolds conjecture (Peres and Reynolds [26]) for miscible flooding, splitting the solution for different zones, where the last one is a single-phase compressible region.
- The development of the pressure solution for the miscible three-component displacement problem, considering infinite and finite reservoirs.

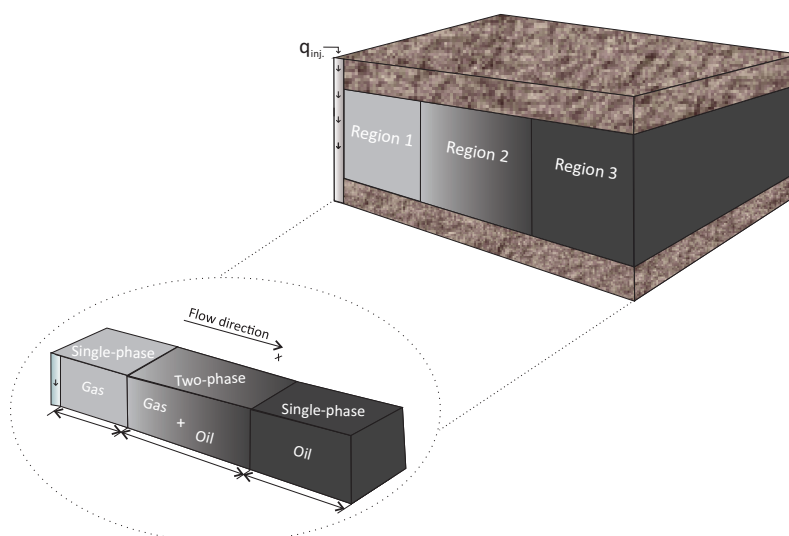


Figure 1. Three-region scheme.

The next section states the problem, the hypotheses used and the mathematical formulation. Then, the solutions for the saturation, component concentrations and pressure are presented. After that, the results for an example based on typical rock–fluid data are shown.

2. Physical and Mathematical Model

This work analyzes the saturation and pressure behavior of one-dimensional isothermal oil displacement by miscible gasflooding at a constant injection rate. The reservoir is considered homogeneous with a constant cross-sectional area and initially filled with oil. Our model considers a two-phase flow of a three-component fluid with instantaneous phase equilibrium. The additional hypotheses are as follows: (1) there are no adsorption and chemical reactions; (2) the pure component density is independent of the phase;

(3) gravitational, dispersion and capillary effects are neglected; and (4) Amagat and Darcy’s laws are valid.

The mass conservation for an n -component system under these hypotheses is given by the following:

$$\frac{\partial}{\partial t} \left(\phi \sum_{j=1}^{N_p} \rho_j s_j w_{ij} \right) + \frac{\partial}{\partial x} \left(\sum_{j=1}^{N_p} \rho_j w_{ij} u_j \right) = 0, \quad i = 1, 2, \dots, N_c, \quad (1)$$

where N_p is the number of phases, N_c is the number of components, t is time, x is the spatial variable, ρ_j is the density of phase j , s_j is the saturation of phase j , u_j is the velocity of phase j , w_{ij} is the mass fraction of component i in phase j and ϕ is the porosity.

If the pure component density is the same for all phases, the mass conservation equation for component i as a function of its volume fraction in phase j can be rewritten using the following relationship:

$$\rho_j w_{ij} = \rho_i c_{ij}, \quad (2)$$

where c_{ij} is the volume fraction of component i in phase j and ρ_i is the pure component density at the system pressure (p) and temperature (T).

The macroscopic phase velocity can be expressed in terms of the fractional flow function (f_j) by the following:

$$f_j = \frac{u_j}{u_T} \Leftrightarrow u_j = f_j u_T, \quad (3)$$

where the total velocity u_T is given by the following:

$$u_T(x, t) = -k \left[\sum_{j=1}^{N_p} \frac{k_{rj}(s_j)}{\mu_j(\vec{C})} \right] \frac{\partial p}{\partial x}, \quad (4)$$

and k is the absolute permeability, k_{rj} is the relative permeability of phase j , μ_j is the viscosity of phase j , \vec{C} is the concentration vector and p is the pressure.

The term inside the brackets in Equation (4) is the total mobility (λ_T); so, this equation can be written as follows:

$$u_T = -\lambda_T(s_j, \vec{C}) k \frac{\partial p}{\partial x}. \quad (5)$$

Applying Equations (2) and (3) in Equation (1), the mass conservation for the i -component becomes the following:

$$\phi \frac{\partial}{\partial t} \left(\sum_{j=1}^{N_p} \rho_i s_j c_{ij} \right) + \frac{\partial}{\partial x} \left(\sum_{j=1}^{N_p} \rho_i c_{ij} u_T f_j \right) = 0, \quad i = 1, 2, \dots, N_c. \quad (6)$$

When the cross-sectional area open to flow is constant, the total velocity is a function of time only. In addition to that, as it is considered that the density of a pure component is constant in all phases, Equation (6) can be rewritten as follows:

$$\phi \frac{\partial}{\partial t} \left(\sum_{j=1}^{N_p} s_j c_{ij} \right) + u_T \frac{\partial}{\partial x} \left(\sum_{j=1}^{N_p} c_{ij} f_j \right) = 0, \quad i = 1, 2, \dots, N_c. \quad (7)$$

The total concentration (C_i) and total flow (F_i) of component i are given by the following:

$$C_i = \sum_{j=1}^{N_p} s_j c_{ij}, \quad (8)$$

and

$$F_i = \sum_{j=1}^{N_p} f_j c_{ij}. \tag{9}$$

With these definitions, the hyperbolic system that governs the multiphase multicomponent flow in porous media becomes the following:

$$\frac{\partial C_i}{\partial t} + \frac{u_T}{\phi} \frac{\partial F_i}{\partial x} = 0, \quad i = 1, 2, \dots, N_c. \tag{10}$$

From the constitutive relations $\sum_{i=1}^{N_c} C_i = \sum_{i=1}^{N_c} F_i = 1$, the number of equations is reduced to $N_c - 1$. Therefore, the hyperbolic system for two-phase three-component flow is reduced to the following system of two equations:

$$\begin{cases} \frac{\partial C_2}{\partial t} + \frac{u_T}{\phi} \frac{\partial F_2}{\partial x} = 0, \\ \frac{\partial C_3}{\partial t} + \frac{u_T}{\phi} \frac{\partial F_3}{\partial x} = 0. \end{cases} \tag{11}$$

3. Solution of the Problem

The solution procedure for phase saturations, concentration and pressure are developed in this section. First, we introduce two auxiliary variables to represent the thermodynamic equilibria. Next, the hyperbolic system is rewritten as a function of these new variables and recast in dimensionless spatial and time variables. Finally, the hyperbolic problem is solved by the method of characteristics.

The solution of the hyperbolic system given by Equation (11) depends on the phase equilibrium conditions at the system pressure and temperature. In this case, it is modeled by a ternary phase diagram [49]. The lines connecting the bubble and dew points in a ternary diagram define the vapor (V) and liquid (L) phase composition at equilibrium. Those lines are known as tie-lines [4] and can be parameterized by two thermodynamic geometric variables α and β (Figure 2), which are given by the following:

$$\alpha = \frac{c_{2o} - c_{2g}}{c_{3o} - c_{3g}} \tag{12}$$

and

$$\beta = c_{2g} - \alpha c_{3g}. \tag{13}$$

The subscripts o and g denote the oil and the gas phases, respectively. The variable α represents the tie-line slope, whereas the β values are the intercept of the tie-line extrapolation with a vertical axis. The tie-lines never intercept each other inside the two-phase region and they can be uniquely identified by a single parameter. In this work, we chose the β variable to represent all the tie-lines.

Using thermodynamic variables, we rewrite the total concentration and total flow of the second component as follows:

$$C_2 = \alpha C_3 + \beta \tag{14}$$

and

$$F_2 = \alpha F_3 + \beta. \tag{15}$$

Applying Equations (14) and (15) in Equation (11), we obtain the following:

$$\begin{cases} \frac{\partial C_3}{\partial t} + \frac{u_T}{\phi} \frac{\partial F_3}{\partial x} = 0, \\ \frac{\partial(\alpha C_3 + \beta)}{\partial t} + \frac{u_T}{\phi} \frac{\partial(\alpha F_3 + \beta)}{\partial x} = 0. \end{cases} \quad (16)$$

The dimensionless time (t_D) and spatial coordinate (x_D) variables are defined by the following:

$$x_D = \frac{x}{L_C} \quad (17)$$

and

$$t_D = \frac{\int_0^t u_T(\tau) d\tau}{\phi L_C}, \quad (18)$$

where L_C is a reservoir characteristic dimension. If the reservoir is finite, L_C corresponds to the reservoir length, i.e., $L_C = L$. If the reservoir is assumed infinite, L_C takes the value of the reservoir width, i.e., $L_C = W$.

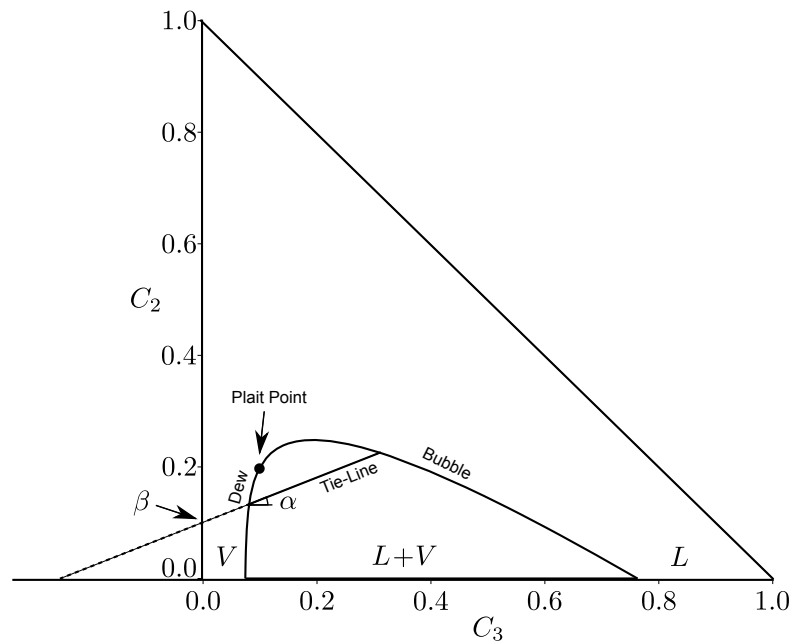


Figure 2. Schematic ternary diagram with thermodynamic geometric variables.

Applying Equations (17) and (18) in Equation (16), the dimensionless hyperbolic system for a three-component two-phase system is as follows:

$$\begin{cases} \frac{\partial C_3}{\partial t_D} + \frac{\partial F_3}{\partial x_D} = 0, \\ \frac{\partial(\alpha C_3 + \beta)}{\partial t_D} + \frac{\partial(\alpha F_3 + \beta)}{\partial x_D} = 0, \end{cases} \quad (19)$$

where $F_3 = F_3(C_3, \beta)$ and $\alpha = \alpha(\beta)$. The initial and boundary conditions are given by the following:

$$\begin{cases} C_3(x_D, t_D = 0) = C_3^{(I)}, & \beta(x_D, t_D = 0) = \beta^{(I)}, \\ C_3(x_D = 0, t_D) = C_3^{(I)}, & \beta(x_D = 0, t_D) = \beta^{(I)}, \end{cases} \quad (20)$$

where $C_3^{(I)}$ and $\beta^{(I)}$ denote, respectively, the total concentration of the third component and the tie-line intercept of the fluid that initially saturates the porous media. The third component total concentration and the tie-line intercept of the injected gas at the inlet point are represented by $C_3^{(J)}$ and $\beta^{(J)}$, respectively.

Expanding Equation (19) leads to the following:

$$\begin{cases} \frac{\partial C_3}{\partial t_D} + \frac{\partial F_3}{\partial C_3} \frac{\partial C_3}{\partial x_D} + \frac{\partial F_3}{\partial \beta} \frac{\partial \beta}{\partial x_D} = 0, \\ \frac{\partial \beta}{\partial t_D} + \left(\frac{\frac{\partial \alpha}{\partial \beta} F_3 + 1}{\frac{\partial \alpha}{\partial \beta} C_3 + 1} \right) \frac{\partial \beta}{\partial x_D} = 0. \end{cases} \tag{21}$$

The hyperbolic system can be recast as follows:

$$\frac{\partial u}{\partial t_D} + A \frac{\partial u}{\partial x_D}, \tag{22}$$

where the vector u and the 2×2 matrix A are given, respectively, by the following:

$$u = \begin{pmatrix} C_3 \\ \beta \end{pmatrix} \tag{23}$$

and

$$A = \begin{bmatrix} \frac{\partial F_3}{\partial C_3} & \frac{\partial F_3}{\partial \beta} \\ 0 & \frac{F_3 \frac{\partial \alpha}{\partial \beta} + 1}{C_3 \frac{\partial \alpha}{\partial \beta} + 1} \end{bmatrix}. \tag{24}$$

The main diagonal elements of the upper triangular matrix A are the eigenvalues of the hyperbolic system, with eigenpairs given by the following:

$$\lambda_C = \frac{\partial F_3}{\partial C_3}, \quad r_C = \begin{pmatrix} 1 \\ 0 \end{pmatrix}, \tag{25}$$

$$\lambda_\beta = \frac{F_3 \frac{\partial \alpha}{\partial \beta} + 1}{C_3 \frac{\partial \alpha}{\partial \beta} + 1}, \quad r_\beta = \begin{pmatrix} -\frac{\partial F_3}{\partial \beta} \\ \frac{\partial F_3}{\partial C_3} - \frac{F_3 \frac{\partial \alpha}{\partial \beta} + 1}{C_3 \frac{\partial \alpha}{\partial \beta} + 1} \end{pmatrix}. \tag{26}$$

The Riemman invariants of the problem are as follows:

$$R_C = F_3 - \int \left(\frac{F_3 \frac{\partial \alpha}{\partial \beta} + 1}{C_3 \frac{\partial \alpha}{\partial \beta} + 1} - \frac{\partial F_3}{\partial C_3} \right) dC_3, \quad R_\beta = \beta. \tag{27}$$

Rarefaction waves calculated from the right eigenvectors are given by the following:

$$\frac{d\beta}{dC_3} = 0 \Rightarrow \beta = R_\beta \tag{28}$$

and

$$\frac{d\beta}{dC_3} = \left(\frac{F_3 \frac{\partial \alpha}{\partial \beta} + 1}{C_3 \frac{\partial \alpha}{\partial \beta} + 1} - \frac{\partial F_3}{\partial C_3} \right) \Rightarrow \beta = \int \left(\frac{F_3 \frac{\partial \alpha}{\partial \beta} + 1}{C_3 \frac{\partial \alpha}{\partial \beta} + 1} - \frac{\partial F_3}{\partial C_3} \right) dC_3 + R_C. \quad (29)$$

The total concentration C_3 changes while the tie-line geometric variable β remains constant along the first rarefaction wave (tie-line path). In the second rarefaction family, both β and C_3 vary (non-tie-line path).

The shock expressions for this problem are found by applying the Rankine–Hugoniot conditions in Equation (19):

$$\begin{cases} [C_3]D = [F_3] \\ [\alpha C_3 + \beta]D = [\alpha F_3 + \beta] \end{cases}, \quad (30)$$

where the notation $[B] = B^+ - B^-$ is used to represent the jump between the right and the left states of the shock of the dummy variable B . Thus, $[B]$ represents the jump of the $[C_3]$, $[F_3]$ and $[\beta]$ variables.

When β is equal in both sides of the shock, i.e., only the concentration changes, the shock wave speed is as follows:

$$D_C = \frac{[F_3]}{[C_3]}, \quad (31)$$

whereas if β changes across the shock, the shock speed is given by the following:

$$D_\beta = \frac{F_3^+ + \frac{[\beta]}{[C_3]}}{C_3^+ + \frac{[\beta]}{[C_3]}} = \frac{F_3^- + \frac{[\beta]}{[C_3]}}{C_3^- + \frac{[\beta]}{[C_3]}}. \quad (32)$$

The solution of the hyperbolic system for an injection fluid with fixed composition and initial constant composition for a given fractional flow curve yields the saturation and phase composition profiles along the porous media. From this solution, the total mobility λ_T spatial profile can be calculated for any dimensionless time. Then, the pressure drop across the porous media can be obtained by a straightforward integration of Darcy’s law over the spatial coordinate [26].

For the constant gas injection flow rate at the inlet point ($x = 0$), the inner boundary condition is given by the following:

$$A \frac{kk_{rg}^{s_{or}}}{\mu_{g,i}^{(j)}} \frac{\partial p}{\partial x} \Big|_{x=0} = -q_{g,sc} B_{g,i}, \quad (33)$$

where $A = Wh$ is the cross-sectional area, s_{or} is the residual oil saturation and $\mu_{g,i}^{(j)}$ and $B_{g,i}$ represent, respectively, the gas viscosity and the gas formation volume factor evaluated with injected gas properties at the system initial pressure. The term $q_{g,sc}$ denotes a constant volumetric gas injection rate at standard conditions. In this work, $q_{g,sc} > 0$ indicates gas injection.

The external boundary condition is defined as pressure maintenance at the point ($x = L$), expressed by the following:

$$p(x = L, t) = p_i. \quad (34)$$

For an infinite porous media, the external boundary condition is as follows:

$$\lim_{x \rightarrow \infty} p(x, t) = p_i, \tag{35}$$

where p_i is the initial pressure. Integrating Equation (5) from a given position x to the external boundary x_s leads to the following:

$$\int_x^{x_s} \frac{\partial p(x', t)}{\partial x'} dx' = - \int_x^{x_s} \frac{q_T(x', t)}{k(x')A(x')} \frac{1}{\lambda_T(x', t)} dx', \tag{36}$$

where $x_s = L$ if the reservoir is finite and $x_s \rightarrow \infty$ if the reservoir is infinite. The term q_T represents the total volumetric flow rate at a given (x, t) .

For a homogeneous reservoir with a constant cross-sectional area, and using the external boundary condition (either Equation (34) or (35)), Equation (36) becomes the following:

$$p(x, t) - p_i = \frac{1}{kA} \int_x^{x_s} \frac{q_T(x', t)}{\lambda_T(x', t)} dx'. \tag{37}$$

The dimensionless pressure variable is defined by the following:

$$p_D = \frac{kk_{ro}^{s_{wi}} A}{q_{g,sc} B_{g,i} \mu_{o,i} L_C} \Delta p, \tag{38}$$

where $\Delta p = p(x, t) - p_i$, s_{wi} denotes the irreducible water saturation and $\mu_{o,i}$ is the oil viscosity at initial pressure.

In dimensionless variables, Equation (37) becomes the following:

$$p_D(x_D, t_D) = \int_{x_D}^{x_{Ds}} \frac{q_D(x'_D, t_D)}{\lambda_{TD}(x'_D, t_D)} dx'_D, \tag{39}$$

where $x_{Ds} = 1$ if the reservoir is finite and $x_{Ds} \rightarrow \infty$ if the reservoir is infinite. In Equation (39), q_D represents the dimensionless volumetric flow rate given by the following:

$$q_D(x_D, t_D) = \frac{q_T(x, t)}{q_{g,sc} B_{g,i}}, \tag{40}$$

whereas λ_{TD} is the dimensionless total mobility defined as follows:

$$\lambda_{TD}(x_D, t_D) = \left(\frac{k_{ro}(s_o)}{\mu_o(\vec{C})} + \frac{k_{rg}(s_o)}{\mu_g(\vec{C})} \right) \frac{\mu_{o,i}}{k_{ro}^{s_{wi}}}. \tag{41}$$

Note that Equation (39) is general, and no assumptions were made about the nature of the mass transfer (miscible or immiscible) between the injected and the original reservoir fluid.

4. Example

This section presents an application of the solution described in the previous section for a specific set of rock and fluid properties (Table 1). The molar fractions (z), critical properties (pressure p_c and temperature T_c), molecular mass (M_w) and acentric factors (w) of the components present in the fluid are given in Table 2 and the fluid concentration at the initial and injection states is shown in Table 3.

Table 1. Rock and fluid physical properties.

Property	Symbol	Value	Unit
System pressure	p	200	bar
System temperature	T	338	K
Oil viscosity at initial conditions	$\mu_{o,i}$	2.75	cp
Residual oil saturation	s_{or}	0.2	-
Irreducible water saturation	s_{wi}	0.0	-
Oil phase endpoint relative permeability	$k_{ro}^{s_{wi}}$	1.0	-
Corey's exponent for the oil phase	n_o	1.8	-
Gas viscosity at injection conditions	$\mu_{g,i}^{(J)}$	0.0402	cp
Critical gas saturation	s_{gc}	0.0	-
Gas phase endpoint relative permeability	$k_{rg}^{s_{or}}$	0.8	-
Corey's exponent for the gas phase	n_g	2.2	-

Table 2. Component thermodynamic properties.

Component	z	T_c (K)	p_c (bar)	M_w (g/mol)	ω
Comp. 1	0.5645	4.1659×10^2	4.5929×10^1	2.2116×10^1	4.4540×10^{-2}
Comp. 2	0.3093	9.8297×10^2	3.0173×10^1	1.0361×10^2	3.3989×10^{-1}
Comp. 3	0.1262	1.4952×10^3	1.3663×10^1	3.4442×10^2	1.0164×10^0

Table 3. Molar composition of the initial and injected fluids.

	Comp. 1	Comp. 2	Comp. 3	C_3	β
Initial Fluid	0.0000	0.0982	0.9018	0.9650	0.0071
Injected Fluid	0.9899	0.0101	0.0000	0.0000	0.0128

To determine the thermodynamic equilibrium of the component system parameterized by the geometric variables (α, β) , it is necessary to construct the binodal curve for a fixed temperature and pressure pair. The volumetric fractions of the liquid (l) and gas (g) phases at equilibrium for a given global composition (z) are obtained through a series of flash calculations, varying the composition while keeping the temperature and pressure constant.

In this example, the thermodynamic equilibrium was calculated using the Peng–Robinson equation of state [50]. Figure 3 shows the binodal curve obtained for 200 bar and 338 K. The tie-line equation was found through a polynomial fit of the calculated geometric variable pairs (α, β) :

$$\alpha(\beta) = 44.057\beta^2 + 3.2102\beta. \tag{42}$$

The relative permeability curves were calculated using Corey's model [51]:

$$\begin{cases} k_{ro} = k_{ro}^{s_{wi}} \left(\frac{s_o - s_{or}}{1 - s_{wi} - s_{or}} \right)^{n_o} \\ k_{rg} = k_{rg}^{s_{or}} \left(\frac{s_g - s_{gc}}{1 - s_{wi} - s_{or}} \right)^{n_g} \end{cases}, \tag{43}$$

where $k_{ro}^{s_{wi}}$ and $k_{rg}^{s_{or}}$ are the oil and gas relative permeability endpoints, s_o and s_g are the oil and gas saturations and n_o and n_g are Corey's exponent of each phase. Figure 4 shows the gas and oil phase relative permeability curves for the data presented in Table 1.

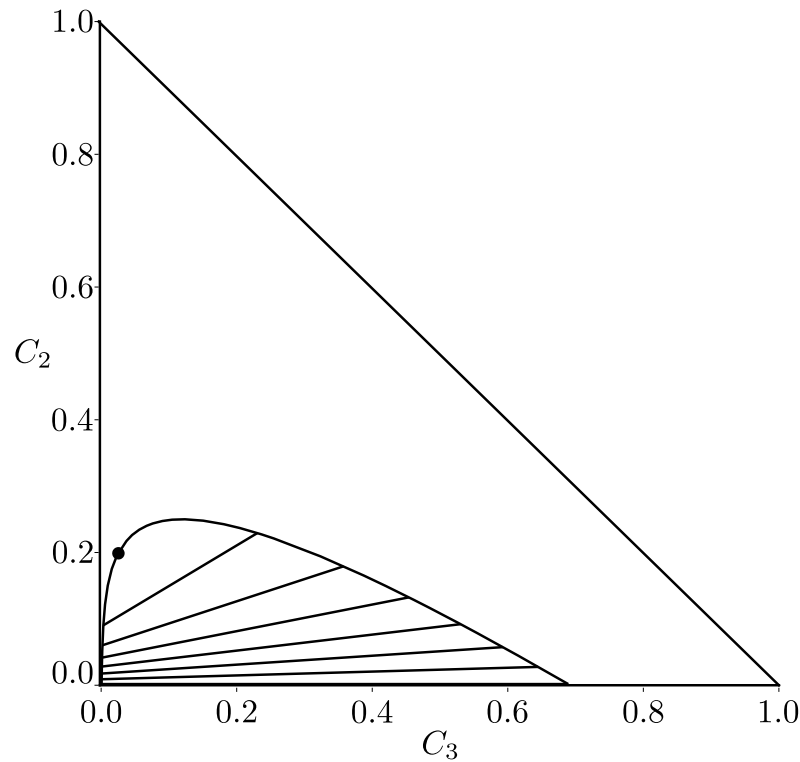


Figure 3. Ternary diagram for the fluid at 200 bar and 338 K.

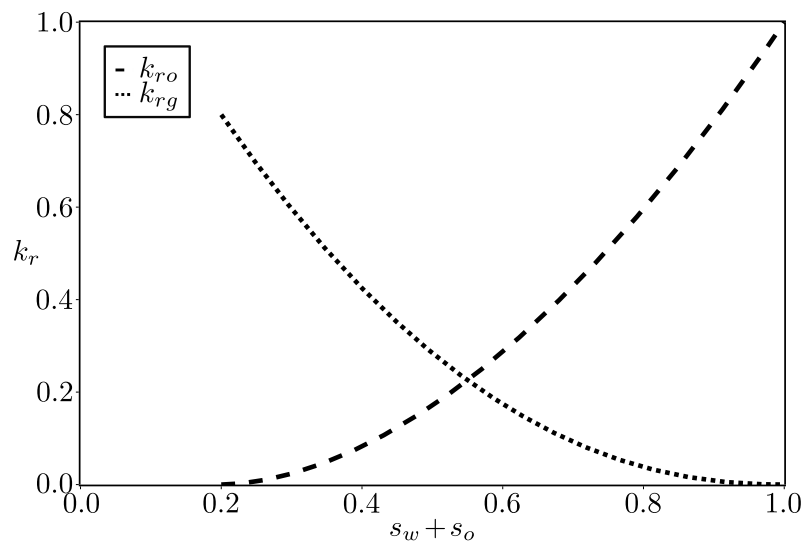


Figure 4. Relative permeability curves for the data shown in Table 1.

The system given by Equation (21) was solved by the method of characteristics for saturation and concentration. The solution path is shown in Figure 5 and is given by $(J) \rightarrow (1) - (2) \rightarrow (3) - (F) \rightarrow (I)$, where the symbols \rightarrow and $-$ denote, respectively, the shock and rarefaction waves and (1), (2), (3) and (F) represent the intermediate states between the injection and initial conditions. The solution path begins at injection conditions (J), which corresponds to single-phase gas (region 1), which is connected to point (1) in the two-phase region (region 2) through a concentration shock. As shown by Bedrikovetsky [52], the transition from single phase to two phase or from two phase to single phase is always made by a concentration shock. From point (1), there is a concentration rarefaction up to point (2). Next, there is a concentration and β shock linking points (2) and (3). From

(3), there is another concentration rarefaction wave up to (F), which is connected to initial condition (I) through a concentration shock. The solution is given by the following:

$$\begin{aligned}
 \begin{matrix} C_3(x_D, t_D) \\ \beta(x_D, t_D) \\ s_g(x_D, t_D) \end{matrix} &= \begin{cases} C_3^{(J)}, \beta^{(J)}, s_g^{(J)}, & 0 < \frac{x_D}{t_D} < D_C = 6.594E - 3, \\ C_3^{(1R)}, \beta^{(J)}, s_g^{(1R)}, & D_C < \frac{x_D}{t_D} < D_\beta = 0.420, \\ C_3^{(1)} = 0.470, \beta^{(I)}, s_g^{(1)} = 0.272, & D_\beta < \frac{x_D}{t_D} < F_C^{(1)} = 0.764, \\ C_3^{(2R)}, \beta^{(I)}, s_g^{(2R)}, & F_C^{(1)} < \frac{x_D}{t_D} < D_{BL} = 1.882, \\ C_3^{(I)}, \beta^{(I)}, s_g^{(I)}, & \frac{x_D}{t_D} > D_{BL} = 1.882, \end{cases} \quad (44)
 \end{aligned}$$

where $F_C^{(1)} = \left(\frac{\partial F_3}{\partial C_3}\right)^{(1)}$ and the *BL* subscript represent a Buckley–Leverett shock type [7]. Furthermore, $C_3^{(iR)}$ and $s^{(iR)}$ represent the concentration and saturation changes along the *i*-th concentration rarefaction wave. The solution path can be seen in Figure 5 and the concentration, saturation and β profiles in Figure 6.

The miscible solution just described is compared to an equivalent immiscible problem for the same rock and fluid properties, given by the following:

$$s_g(x_D, t_D) = \begin{cases} s_g^{(J)}, & \frac{x_D}{t_D} = 0, \\ s_g^{(1R)}, & 0 < \frac{x_D}{t_D} < D_{BL(immis.)} = 4.472, \\ s_g^{(I)}, & D_{BL(immis.)} < \frac{x_D}{t_D}, \end{cases} \quad (45)$$

where $s_g^{(1R)}$ represents the gas saturation along the immiscible rarefaction wave. The gas saturation profiles for miscible and immiscible solutions are compared in Figure 7. Note that the gas front of the miscible solution is slower than the immiscible one.

Equation (39) can be used to compute the dimensionless pressure at the injection point ($x_D = 0$) for any dimensionless time once the saturation and concentration profiles are calculated. As the single-phase gas region 1 is very small, it can be neglected; thus, Equation (39) yields the following:

$$\begin{aligned}
 p_D(x_D = 0, t_D) &= p_{wD}(t_D) = \int_0^{D_\beta t_D} \frac{q_D(x'_D, t_D)}{\lambda_{TD}^{(2a)}(x'_D, t_D)} dx'_D \\
 &+ \int_{D_\beta t_D}^{x_{DF}} \frac{q_D(x'_D, t_D)}{\lambda_{TD}^{(2b)}(x'_D, t_D)} dx'_D + \int_{x_{DF}}^{D_{BL} t_D} \frac{q_D(x'_D, t_D)}{\lambda_{TD}^{(2c)}(x'_D, t_D)} dx'_D \\
 &+ \int_{D_{BL} t_D}^{x_{Ds}} \frac{q_D(x'_D, t_D)}{\lambda_{TD}^{(3)}(x'_D, t_D)} dx'_D. \quad (46)
 \end{aligned}$$

where $x_{DF} = F_C^{(1)} t_D$. The superscript in the dimensionless total mobility variable λ_{TD} denotes the saturation region. Note that the integration is split according to the rarefaction and constant states: the two-phase region ($0 < x_D < D_{BL} t_D$) is sub-divided into a rarefaction-region 2a ($0 < x_D < D_\beta t_D$), a constant-state region 2b ($D_\beta t_D < x_D < x_{DF}$) and a rarefaction-region 2c ($x_{DF} < x_D < D_{BL} t_D$).

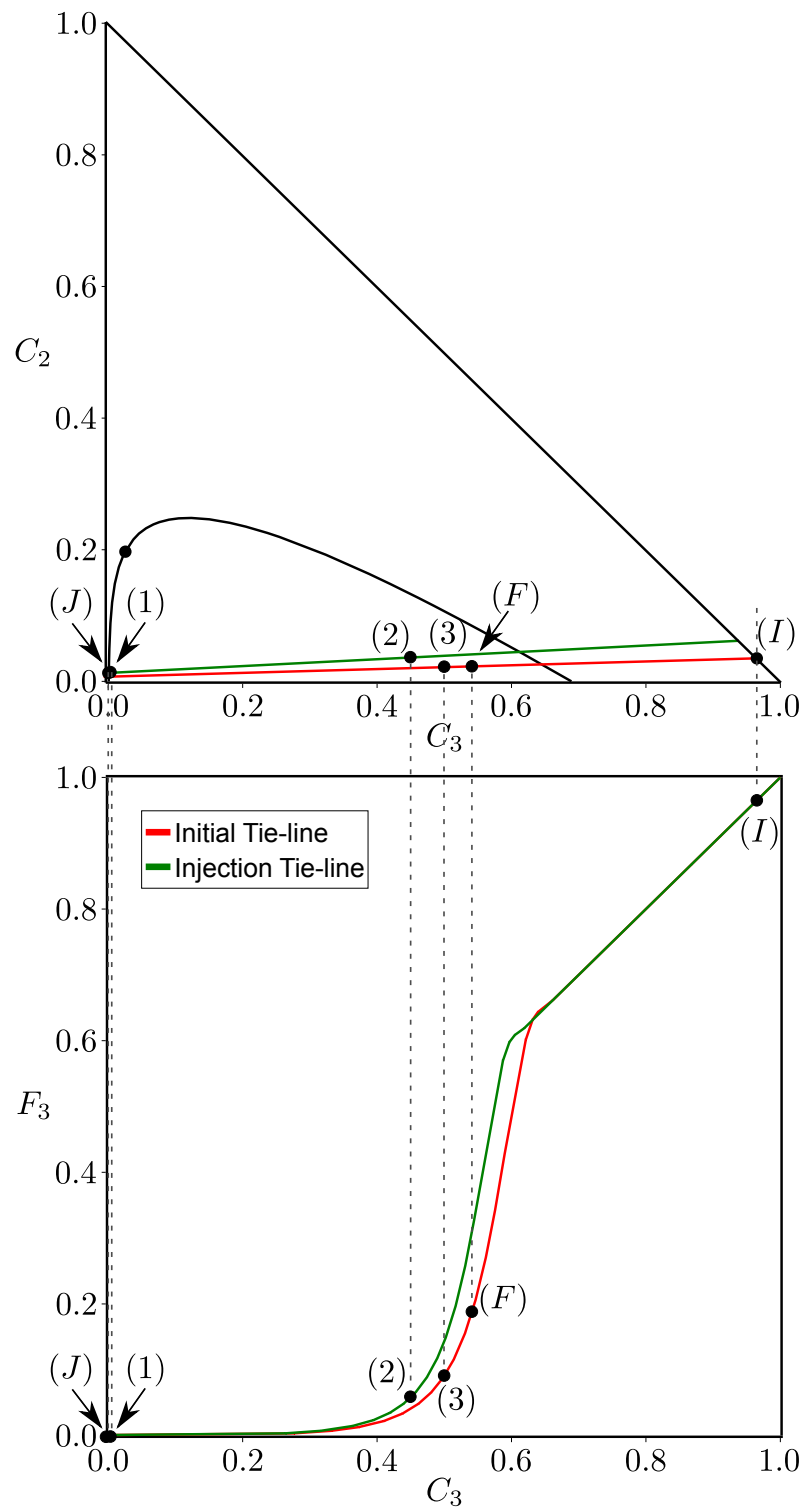


Figure 5. The initial and injection tie-lines and the fractional flow plot.

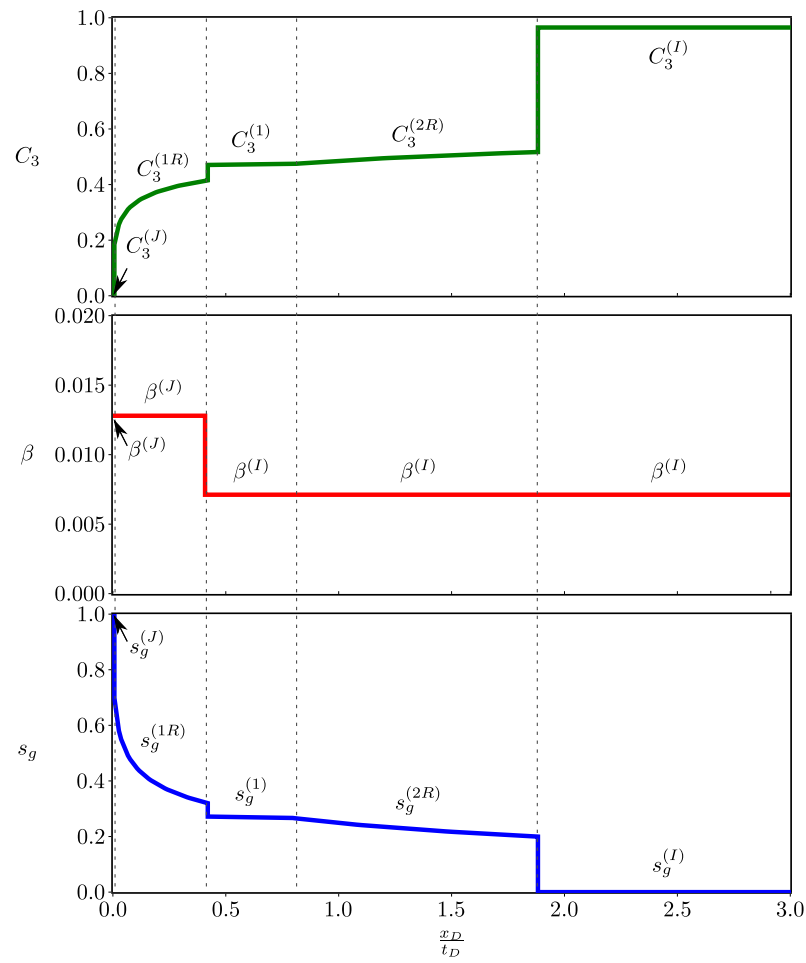


Figure 6. C_3 volumetric concentration, gas saturation and β profiles.

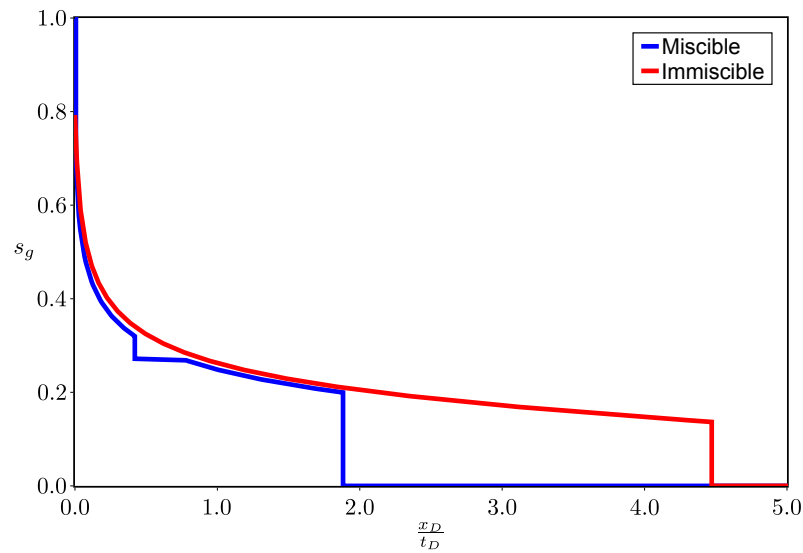


Figure 7. Saturation profile comparison between miscible and immiscible displacements.

We add and subtract the following term:

$$\int_0^{D_{BL}t_D} \frac{q_D(x'_D, t_D)}{\lambda_{TD}^{(3)}(x'_D, t_D)} dx'_D,$$

Equation (46) becomes the following:

$$\begin{aligned}
 p_{wD}(t_D) = & \int_0^{D_{\beta}t_D} q_D(x'_D, t_D) \left(\frac{1}{\lambda_{TD}^{(2a)}(x'_D, t_D)} - \frac{1}{\lambda_{TD}^{(3)}(x'_D, t_D)} \right) dx'_D \\
 & + \int_{D_{\beta}t_D}^{x_{DF}} q_D(x'_D, t_D) \left(\frac{1}{\lambda_{TD}^{(2b)}(x'_D, t_D)} - \frac{1}{\lambda_{TD}^{(3)}(x'_D, t_D)} \right) dx'_D \\
 & + \int_{x_{DF}}^{D_{BL}t_D} q_D(x'_D, t_D) \left(\frac{1}{\lambda_{TD}^{(2c)}(x'_D, t_D)} - \frac{1}{\lambda_{TD}^{(3)}(x'_D, t_D)} \right) dx'_D + \int_0^{x_{Ds}} \frac{q_D(x'_D, t_D)}{\lambda_{TD}^{(3)}(x'_D, t_D)} dx'_D. \quad (47)
 \end{aligned}$$

Assuming that the two-phase region is located within the steady-state region, we have $q_D(x_D, t_D) = 1$ for $x_D \leq D_{BL}t_D$. Thus, Equation (47) simplifies to

$$\begin{aligned}
 p_{wD}(t_D) = & \int_0^{D_{\beta}t_D} \left(\frac{1}{\lambda_{TD}^{(2a)}(x'_D, t_D)} - 1 \right) dx'_D \\
 & + \left(\frac{1}{\lambda_{TD}^{(2b)}} - 1 \right) (x_{DF} - D_{\beta}t_D) \\
 & + \int_{x_{DF}}^{D_{BL}t_D} \left(\frac{1}{\lambda_{TD}^{(2c)}(x'_D, t_D)} - 1 \right) dx'_D + \int_0^{x_{Ds}} q_D(x'_D, t_D) dx'_D, \quad (48)
 \end{aligned}$$

It was also used that the total mobility in region 2b ($\lambda_{TD}^{(2b)}$) is constant and that, in region 3, $\lambda_{TD}^{(3)}$ is equal to 1.

The first three terms in Equation (48) represent the pressure drop due to the mobility contrast between the injected fluid and the original reservoir fluid. The last term represents the slightly compressible single-phase oil solution, which depends on the external boundary condition, either an infinite or a finite reservoir.

4.1. Infinite-Reservoir Case

It can be shown that the single-phase dimensionless pressure for slightly compressible fluids at $x_D = 0$ (p_{wD0}) for an infinite reservoir ($x_{Ds} \rightarrow \infty$) is given by the following:

$$p_{wD0}(t_D) = \sqrt{\frac{4t_D}{\pi\gamma_L}}, \quad (49)$$

where γ_L is a dimensionless parameter defined by the following:

$$\gamma_L = \frac{\mu_{o,i} c_{t,i} L_C q_{g,sc} B_{g,i}}{kk_{ro}^{s_{wi}} A}. \quad (50)$$

and $c_{t,i}$ is the total compressibility evaluated at the initial pressure. Note that γ_L is directly proportional to the injection rate and thus represents the impact of the flow rate on the saturation and pressure behavior. The pressure derivative taken with respect to the natural logarithm of time, introduced by Bourdet et al. [53], is a useful technique to reveal and diagnose the pressure behavior with time. Thus, the pressure derivative of Equation (49) with respect to the natural logarithm of time yields

$$p'_{wD0}(t_D) = \frac{1}{2} \sqrt{\frac{4t_D}{\pi\gamma_L}}. \quad (51)$$

Equations (49) and (51) show that, in a log–log plot, the single-phase solution and its logarithmic-derivative curves appear as two parallel straight lines with the slope $\frac{1}{2}$ and are displaced by a constant equal to $\log 2$. This is a characteristic feature of the single-phase flow of a slightly compressible fluid in a linear infinite reservoir.

Substituting Equation (49) in the last term of Equation (48), we obtain

$$p_{wD}(t_D) = \int_0^{D\beta t_D} \left(\frac{1}{\lambda_{TD}^{(2a)}(x'_D, t_D)} - 1 \right) dx'_D + \left(\frac{1}{\lambda_{TD}^{(2b)}} - 1 \right) (x_{DF} - D\beta t_D) + \int_{x_{DF}}^{D_{BL}t_D} \left(\frac{1}{\lambda_{TD}^{(2c)}(x'_D, t_D)} - 1 \right) dx'_D + \sqrt{\frac{4t_D}{\pi\gamma_L}}. \quad (52)$$

Figure 8 shows the pressure evolution at the inlet point calculated by Equation (52) for the data presented earlier for $\gamma_L = 0.01848$. For comparison purposes, the single-phase slightly compressible (oil) solution is also plotted in this figure. This plot shows that the injection–solution curve runs below the single-phase solution for all times. This happens for mobility ratios much greater than one, as the displacing fluid mobility (gas) is higher than the displaced fluid (oil). Therefore, the pressure drop at a given time becomes smaller than the pressure drop for a single-phase flow for the same injection rate.

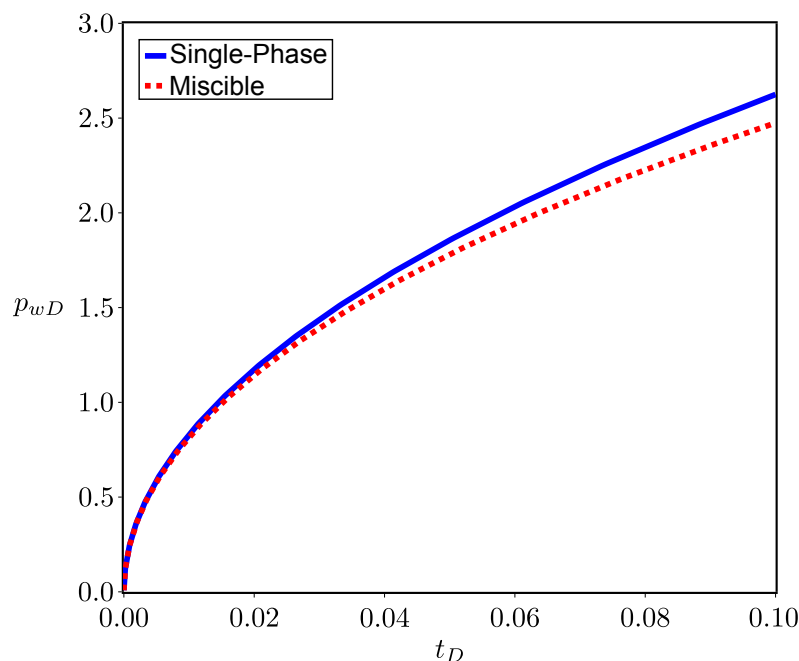


Figure 8. Pressure behavior comparison: single-phase slightly compressible fluid solution (p_{wD0}) and partially miscible solution (p_{wD}) for an infinite reservoir for $\gamma_L = 0.01848$.

The pressure derivative can be very helpful to understand the injectivity problem considered here. A convenient expression is obtained if Equation (52) is rewritten using

the self-similar variable $y = x_D/t_D$, and then the resulting expression with respect to the natural logarithm of time is derived:

$$p'_{wD}(t_D) = t_D \int_0^{D_\beta} \left(\frac{1}{\lambda_{TD}^{(2a)}(y')} - 1 \right) dy' + t_D \left(\frac{1}{\lambda_{TD}^{(2b)}} - 1 \right) (F'_C{}^{(1)} - D_\beta) + t_D \int_{F'_C{}^{(1)}}^{D_{BL}} \left(\frac{1}{\lambda_{TD}^{(2c)}(y')} - 1 \right) dy' + \frac{1}{2} \sqrt{\frac{4t_D}{\pi \gamma_L}}. \quad (53)$$

The first three terms in Equation (53) represent the effect on the derivative caused by the mobility contrast within the two-phase flow region. Figure 9 shows a log–log plot of the dimensionless pressure and its logarithmic derivative with respect to dimensionless time for both injectivity and single-phase solutions for $\gamma_L = 0.01848$. As mentioned before, the single-phase oil solution and its derivative display a straight line with a half slope in a log–log plot. The injectivity test solution and its derivative continuously deviate from their single-phase counterpart. As the mobility ratio is unfavorable in this example ($\hat{M} \approx 55$), the first three terms in Equations (52) and (53) are negative; thus, the injectivity test solution becomes increasingly smaller than the single-phase liquid solution. This implies that if one analyzes this injectivity test data with single-phase equations, the reservoir permeability would be overestimated.

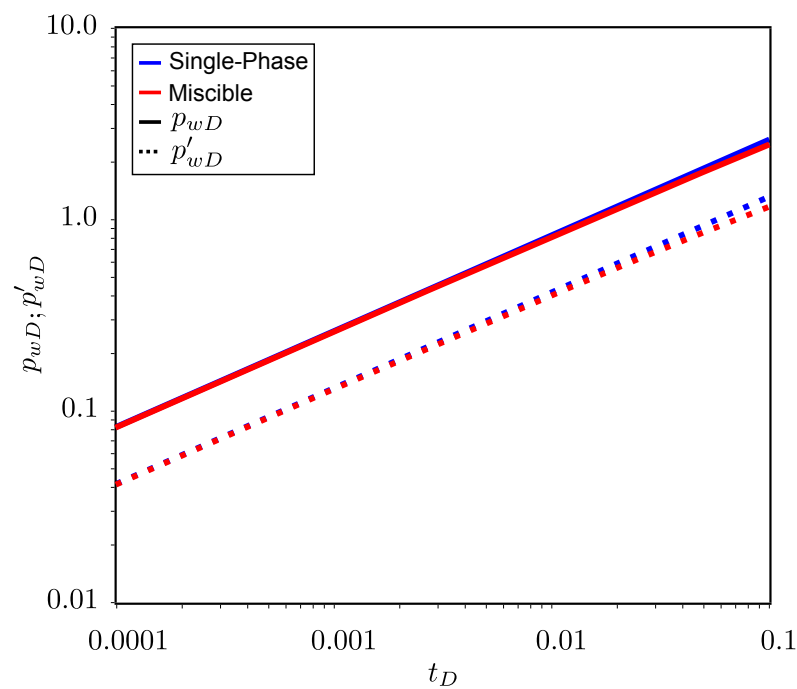


Figure 9. Dimensionless pressure p_{wD} and its derivative p'_{wD} for an infinite reservoir for $\gamma_L = 0.01848$.

Figure 10 shows a dimensionless pressure comparison between miscible and immiscible displacements for the same data of Table 1. The miscible and immiscible solutions show similar behavior; however, the pressure drop for a miscible displacement is greater than the one required by an immiscible displacement for the same injection rate.

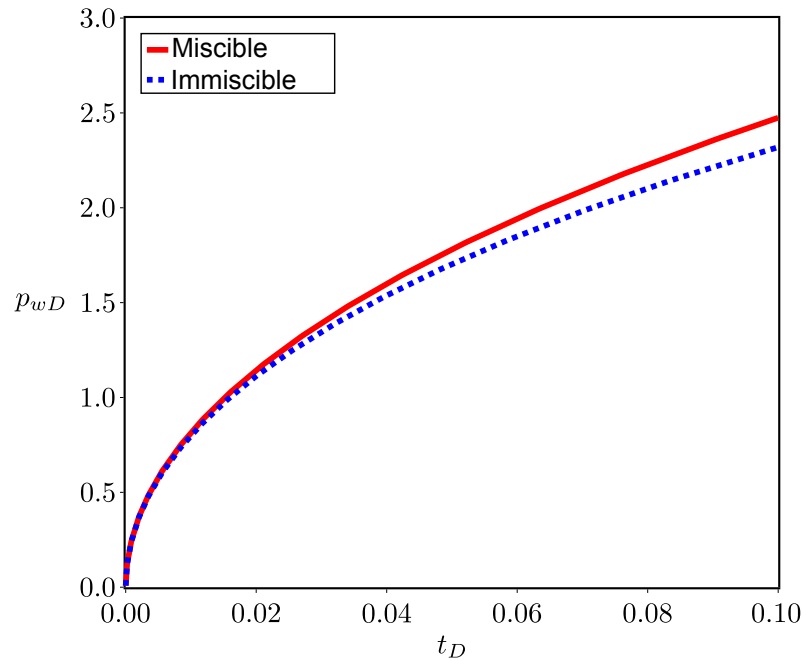


Figure 10. Pressure behavior comparison: miscible and immiscible displacements for an infinite reservoir for $\gamma_L = 0.01848$.

To evaluate the effect of the injection rate on the pressure solution, it is convenient to rewrite (52) using the self-similar variable $y = x_D/t_D$, that is,

$$p_{wD}(\tilde{t}_D, \gamma_L) = \gamma_L \tilde{t}_D \left\{ \int_0^{D_\beta} \left(\frac{1}{\lambda_{TD}^{(2a)}(y')} - 1 \right) dy' + \left(\frac{1}{\lambda_{TD}^{(2b)}} - 1 \right) (F_C^{(1)} - D_\beta) + \int_{F_C^{(1)}}^{D_{BL}} \left(\frac{1}{\lambda_{TD}^{(2c)}(y')} - 1 \right) dy' \right\} + \sqrt{\frac{4\tilde{t}_D}{\pi}}, \quad (54)$$

where $\tilde{t}_D = \frac{t_D}{\gamma_L} = \frac{k k_{ro}^{swi} t}{\mu_{o,i} \phi c_{t,i} L_C^2}$, and $L_C \equiv W$.

Figure 11 presents the dimensionless injection solution p_{wD} versus the dimensionless time \tilde{t}_D for three values of the dimensionless parameter γ_L shown in Table 4. This parameter can be regarded as a dimensionless injection rate. This figure shows that the higher the injection rate, the lower the dimensionless pressure drop for a given dimensionless time \tilde{t}_D , which is consistent with Equation (54). For the unfavorable displacement case considered here ($\tilde{M} \approx 55$), the three terms inside the braces in Equation (54) are negative for all \tilde{t}_D . As these terms are multiplied by γ_L , the p_{wD} solution grows slower for higher γ_L values.

Table 4. Dimensionless parameter γ_L .

γ_L	Value
γ_{L1}	0.00924
γ_{L2}	0.01848
γ_{L3}	0.03696

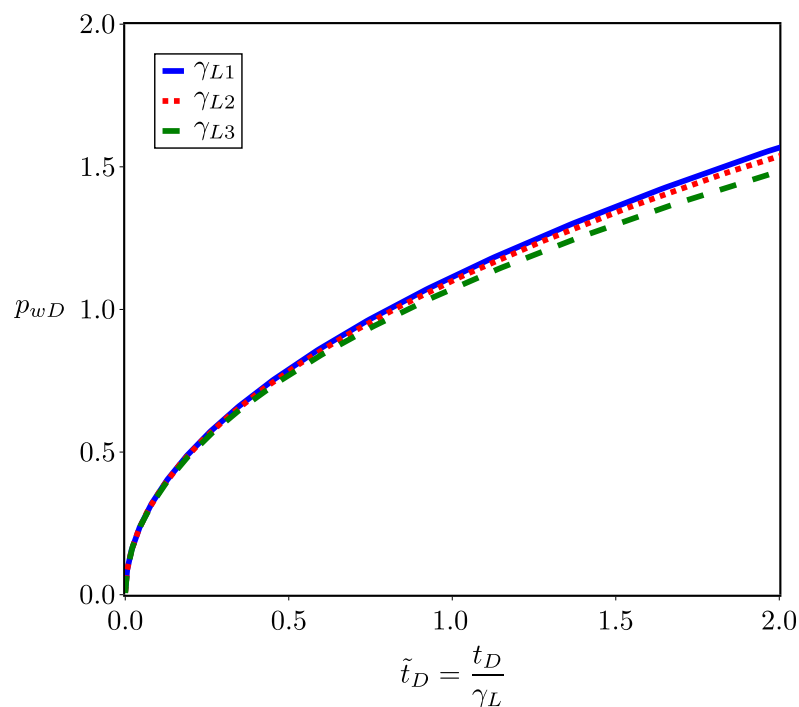


Figure 11. Pressure behavior with respect to the dimensionless parameter γ_L for an infinite reservoir ($\gamma_{L1} < \gamma_{L2} < \gamma_{L3}$).

In this work, the injectivity pressure solution is derived under the assumption that the flood front is always within a steady-state-like region. According to Peres and Reynolds [26], the steady-state region boundary is defined as the position at which the total flow rate changes more rapidly with time. With this definition, the boundary of the steady-state region for one-dimensional linear flow is given by the following:

$$x_{D,ss} = \sqrt{\frac{2t_D}{\gamma_L}}, \tag{55}$$

where $x_{D,ss}$ denotes the steady-state boundary position at a given time.

Thus, we must have the following:

$$x_{D,ss} > D_{BL}t_D. \tag{56}$$

Combining Equations (55) and (56), the pressure solution derived is valid for

$$t_D < \frac{2}{\gamma_L(D_{BL})^2}. \tag{57}$$

For the γ_L values used in this work shown in Table 4, namely, $\gamma_{L1} = 0.00924$, $\gamma_{L2} = 0.01848$ and $\gamma_{L3} = 0.03696$, Equation (57) predicts that the dimensionless pressure solution given by Equation (52) is valid for dimensionless times smaller than 61.1, 30.6 and 15.3, respectively. So, the results presented in Figures 8–11 satisfy the above time criteria.

4.2. Finite-Reservoir Case

The single-phase oil dimensionless solution at $x_D = 0$ (p_{wD0}) for a finite reservoir ($x_{Ds} = 1$) is as follows:

$$p_{wD0}(t_D) = 1 - \frac{8}{\pi^2} \sum_{n=0}^{\infty} \left[\frac{1}{(2n+1)^2} \exp\left(\frac{-(2n+1)^2 \pi^2 t_D}{4\gamma_L}\right) \right]. \tag{58}$$

So, the inlet pressure solution for this case is as follows:

$$p_{wD}(t_D) = \int_0^{D_\beta t_D} \left(\frac{1}{\lambda_{TD}^{(2a)}(x'_D, t_D)} - 1 \right) dx'_D + \left(\frac{1}{\lambda_{TD}^{(2b)}} - 1 \right) (x_{DF} - D_\beta t_D) + \int_{x_{DF}}^{D_{BL} t_D} \left(\frac{1}{\lambda_{TD}^{(2c)}(x'_D, t_D)} - 1 \right) dx'_D + 1 - \frac{8}{\pi^2} \sum_{n=0}^{\infty} \left[\frac{1}{(2n+1)^2} \exp\left(\frac{-(2n+1)^2 \pi^2 t_D}{4\gamma_L}\right) \right]. \tag{59}$$

Equation (59) is valid only for $t_D < \frac{1}{D_{BL}}$, that is, the above solution holds until the injected gas breaks through at $x = L$. The solutions for longer times are given in Appendix A.

The single-phase slightly compressible solution and injection pressure evolution with time at the inlet point for $\gamma_L = 0.01848$ are shown by Figure 12. Initially, the injection pressure behavior is dominated by the single-phase solution p_{wD0} , and, as a consequence, the pressure increases continuously and reaches a maximum value at $t_D \approx 0.031$. Equation (58) shows that $p_{wD0}(t_D)$ tends to 1 at long times. For the data used in this example, the first three terms in Equation (59) are negative; thus, the injection pressure p_{wD} eventually decreases. After the maximum pressure is reached, the pressure declines sharply until the breakthrough ($t_D \approx 0.53$). After that, the pressure solution decreases slowly with three different rates, determined by the $F_C^{(1)}$ point and the β shock (D_β). At long times, the pressure curve flattens out as the gas saturation increases at the outlet.

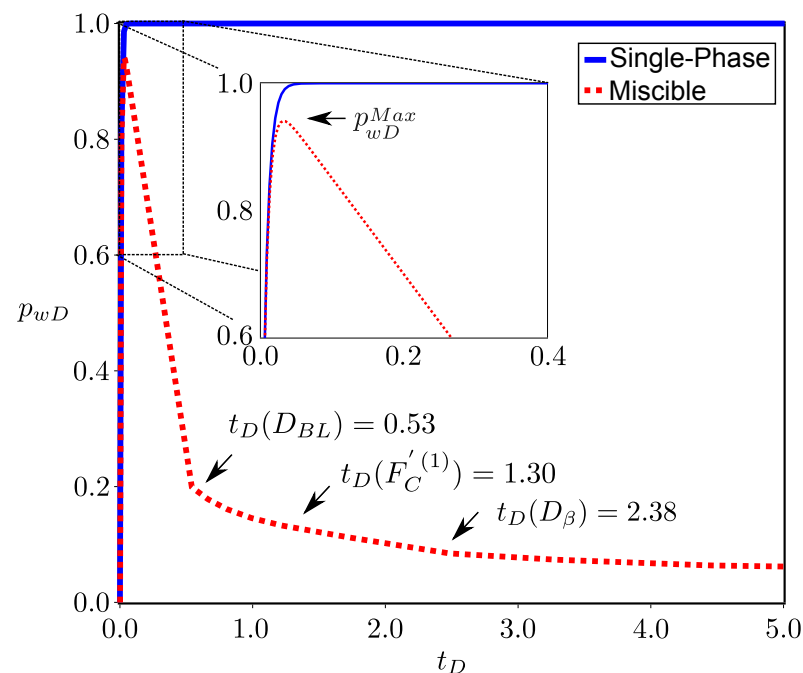


Figure 12. Pressure behavior comparison: single-phase and miscible displacement solutions for a finite reservoir for $\gamma_L = 0.01848$.

The injection pressure derivative with respect to the logarithm of time written as a function of the self-similar variable y is as follows:

$$p'_{wD}(t_D) = t_D \int_0^{D_\beta} \left(\frac{1}{\lambda_{TD}^{(2a)}(y')} - 1 \right) dy' + t_D \left(\frac{1}{\lambda_{TD}^{(2b)}} - 1 \right) (F_C'^{(1)} - D_\beta) + t_D \int_{F_C'^{(1)}}^{D_{BL}} \left(\frac{1}{\lambda_{TD}^{(2c)}(y')} - 1 \right) dy' + \frac{2t_D}{\gamma_L} \sum_{n=0}^{\infty} \left[\exp \left(\frac{-(2n+1)^2 \pi^2 t_D}{4\gamma_L} \right) \right]. \quad (60)$$

Note that Equation (60) holds for $t_D < \frac{1}{D_{BL}}$. Expressions for longer times can be found in Appendix A.

Figure 13 shows the derivative versus time behavior. The single-phase solution becomes a constant at $t_D = 0.07$ and has no effect on the derivative thereafter. From this time until breakthrough ($t_D \approx 0.53$), the pressure derivative becomes a constant. After the breakthrough, the derivative increases due to the arrival of the Buckley–Leverett shock at the outlet.

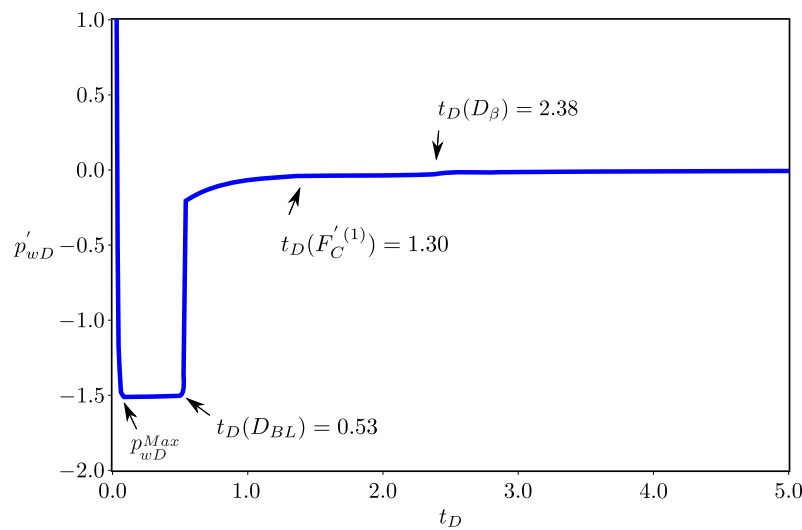


Figure 13. Wellbore dimensionless pressure derivative for a finite reservoir for $\gamma_L = 0.01848$.

Figure 14 shows the pressure solution for the immiscible case for the same data in Table 1. In the immiscible solution, the breakthrough is earlier. Note that the miscible displacement–pressure curve presents more features caused by the different flood fronts arriving at the reservoir outlet.

The effect of the injection rate on the pressure behavior for three γ_L values (Table 4) is shown in Figure 15. As the displacement is not favorable to oil ($\hat{M} \gg 1$), the higher the injection rate, the lower the pressure at a given t_D . The dimensionless pressure maxima occurs earlier for higher rates.

The solution for finite reservoirs derived here (Equation (59) and in Appendix A) are valid when the criteria given by Equation (57) are satisfied. However, it is necessary to check it for times before the steady-state region reaches the reservoir outlet only. From Equation (55), note that $x_{D,ss} = 1$ for $t_D = \gamma_L/2$. Using this t_D value for $x_{D,ss} = 1$ in Equation (56) yields

$$\gamma_L < \frac{2}{D_{BL}} \quad (61)$$

Thus, when Equation (61) is satisfied, the p_{wD} solutions for finite reservoirs are valid for all times. From Equation (44), we see that $D_{BL} = 1.882$, so all γ_L values used in this work (Table 4) satisfy this criteria.

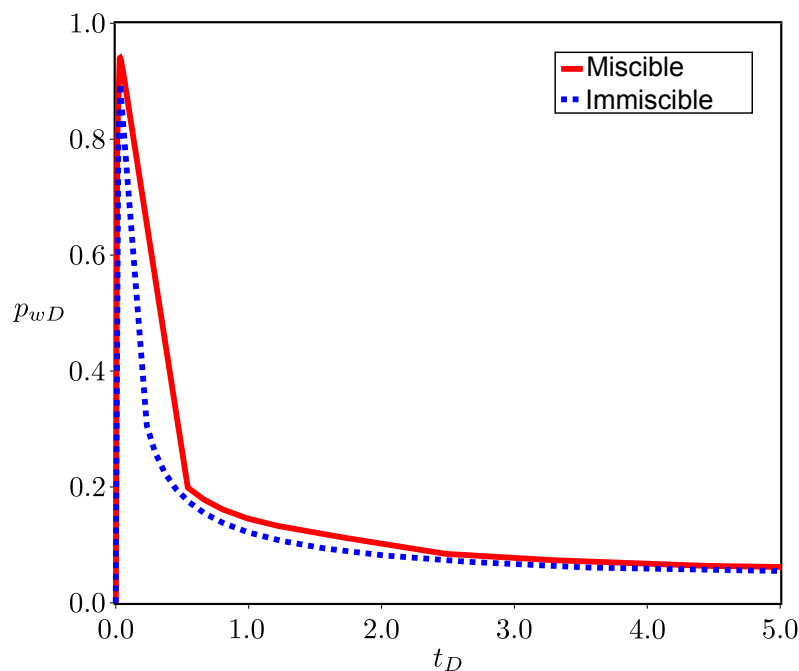


Figure 14. Pressure behavior comparison: miscible and immiscible displacements for a finite reservoir for $\gamma_L = 0.01848$.

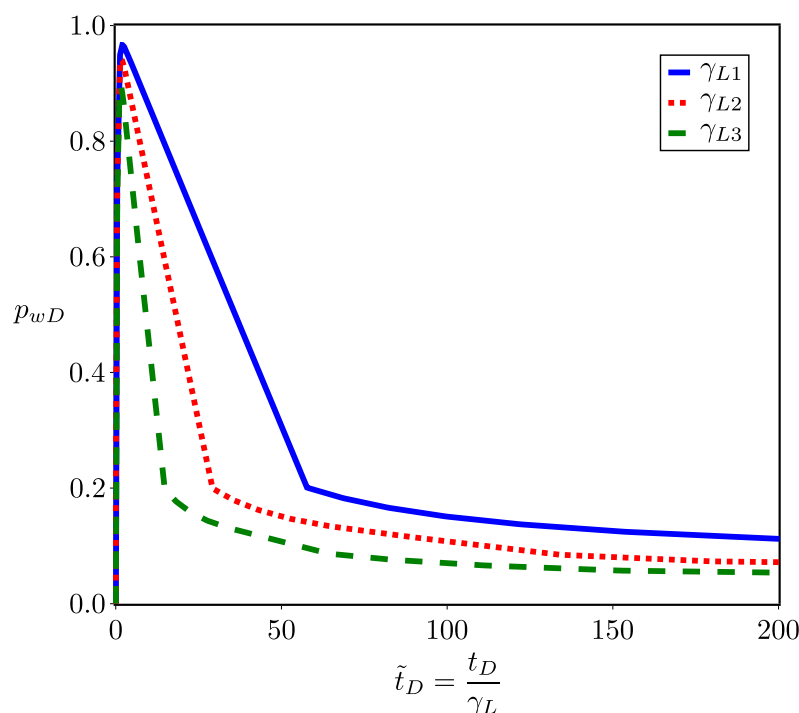


Figure 15. Pressure behavior with respect to the dimensionless parameter γ_L for a finite reservoir ($\gamma_{L1} < \gamma_{L2} < \gamma_{L3}$).

5. Conclusions

This work presents an analytical solution for one-dimensional oil displacement by miscible gas injection at a constant rate of a three-component fluid system in a homogeneous reservoir. The Goursat–Riemann problem for phase saturation and component concentration is given by a system of two hyperbolic equations that is solved by the method of characteristics. The transient pressure solution is obtained by integrating Darcy’s law over the spatial domain once the saturation, composition and total mobility are calculated.

The results for a chosen data set are presented. For this data set, which represents an unfavorable displacement case, the saturation solution shows a two-phase region composed of two rarefaction waves separated by a constant state.

We considered two kinds of external boundary conditions: an infinite reservoir and a finite reservoir with constant external pressure. The first case is representative of an injectivity test conducted in a hydraulically fractured well at the early stages of an EOR project. The second one can be used for screening an improved recovery method for a direct-line-drive pattern. In either case, the pressure solution is given by the sum of two parts: the first one reflects the effect of the mobility contrast between the injected gas and the original reservoir oil; the second term represents the single-phase pressure solution. The injection pressure solution is derived under the assumption that the two-phase region near the injection point is located within a steady-state-like region. We present simple expressions to check the validity of the solutions.

For the infinite-reservoir case, the injection pressure increases continuously with time but is smaller than the correspondent single-phase pressure solution due to the unfavorable mobility ratio. For the example given in this paper, the pressure derivative does not present a straight line with a $1/2$ slope in a log–log plot. Thus, if such injectivity test data are analyzed by single-phase theory, the absolute permeability would be overestimated. For a finite reservoir, the pressure behavior changes as the flood fronts reach the reservoir outlet. At early times, the single-phase solution dominates the pressure behavior at the injection point. At later times, before the injected gas breaks through, the single-phase pressure grows less rapidly as it asymptotically approaches the external pressure, while the term related to the mobility contrast between the fluids becomes increasingly negative. As a result, the injection pressure eventually begins to decrease with time, as expected for an unfavorable displacement. This paper also compares the displacement efficiency and the injection pressure behavior to an equivalent immiscible gas injection.

We also suggest the following points for future research:

- An extension for an n -component system, with the application of the theory described in Pires et al. [19].
- An introduction of the variable injection flow-rate velocity, with the application of Duhamel's principle.
- A sensitivity evaluation of the miscibility effects on Thompson Reynold's conjecture.

Author Contributions: The authors have the following contributions at each step of this work: Conceptualization: L.K.S.S., A.P.P. and A.M.M.P. contributed equally on the conceptualization step. Methodology: The authors contributed equally on this topic. Software, validation and investigation: L.K.S.S. and W.Q.B. contributed equally on the coding and results generation. All the authors contributed equally to the investigation and results validation. Writing and Review: All the authors contributed equally to writing and reviewing this paper. All authors have read and agreed to the published version of the manuscript.

Funding: This study was financed in part by the Coordenação de Aperfeiçoamento de Pessoal de Nível Superior—Brasil (CAPES)—Finance Code 001. Alvaro Peres acknowledges the Universidade Estadual do Norte Fluminense (UENF) for the financial support. The authors also thank Petrobras for funding this research through the SIGER Research Network.

Data Availability Statement: The original contributions presented in this study are included in the article. Further inquiries can be directed to the corresponding author.

Acknowledgments: The authors deeply appreciate the helping hand given by Luana Cantagesso during the preparation of this manuscript.

Conflicts of Interest: The authors declare no conflicts of interest.

Nomenclature

A	Porous media cross-sectional area; matrix of the hyperbolic system
$B_{g,i}$	Gas formation volume factor at initial pressure
\vec{C}	Concentration vector
c_{ij}	Volume fraction of component i in phase j
C_i	Total volumetric concentration of component i
$c_{t,i}$	Total compressibility at initial conditions
D	Shock velocity
F_i	Total flow of component i
f_j	Fractional flow of phase j
k	Porous media absolute permeability
k_{rj}	Relative permeability of phase j
k_{rg}^{sor}	Gas relative permeability at residual oil saturation
k_{ro}^{swi}	Oil relative permeability at irreducible water saturation
L_C	Reservoir characteristic length
L	Reservoir length
\hat{M}	Endpoint mobility ratio; $\hat{M} = [k_{rg}^{sor} / \mu_{g,i}] / [k_{ro}^{swi} / \mu_{o,i}]$
M_w	Molecular weight
N_c	Number of components
N_p	Number of phases
n_j	Corey's exponent of phase j
p_c	Critical pressure
p	System pressure
p_i	Initial pressure
p_{wD}	Wellbore dimensionless injection pressure
p_{wDo}	Wellbore dimensionless injection pressure of the single-phase oil region
$q_{g,sc}$	Constant volumetric gas injection rate at standard conditions
q_T	Total volumetric flow rate
r	Right eigenvector
R	Riemman invariant
s_j	Saturation of phase j
s_{gc}	Critical gas saturation
s_{or}	Residual oil saturation
s_{wi}	Irreducible water saturation
T	Temperature
t	Time coordinate
T_c	Critical temperature
u	Vector of C and β
u_j	Velocity of phase j
u_T	Total velocity
x	Space coordinate
x_s	Porous media external boundary
x_{Ds}	Dimensionless porous media external boundary
$x_{D,ss}$	Dimensionless steady-state boundary
W	Porous media width
w_{ij}	Mass fraction of component i in phase j
z	Molar fraction

Greek characters

α, β	Thermodynamic geometric variable
-----------------	----------------------------------

γ_L	Dimensionless parameter
λ	Characteristic velocities (eigenvalues)
λ_T	Total mobility
μ_j	Viscosity of phase j
$\mu_{g,i}^{(J)}$	Gas viscosity injection at the system initial pressure
$\mu_{o,i}$	Oil viscosity at the system initial pressure
ρ_i	Pure component density at P and T
ρ_j	Density of phase j
ϕ	Porous media porosity
ω	Acentric factor

Subscripts

1,2,3	Components
BL	Buckley–Leverett shock
D	Dimensionless variable
g	Gas phase
i	Component index
j	Phase index
o	Oil phase

Superscript

$(i - R)$	$i - th$ rarefaction wave
(I)	Initial condition
(J)	Injection condition
$-$	Upstream shock state
$+$	Downstream shock state

Appendix A. Dimensionless Solutions for Finite Reservoirs

In this Appendix, the complete solutions for finite reservoirs are presented. Note that the terms in the two-phase regions $2a$, $2b$ and $2c$ are written as a function of the self-similar variable $y = x_D/t_D$.

Appendix A.1. Before Breakthrough: $t_D < \frac{1}{D_{BL}}$

$$\begin{aligned}
 p_{wD}(t_D) = & t_D \int_0^{D_\beta} \left(\frac{1}{\lambda_{TD}^{(2a)}(y')} - 1 \right) dy' + t_D \left(\frac{1}{\lambda_{TD}^{(2b)}} - 1 \right) (F_C'^{(1)} - D_\beta) \\
 & + t_D \int_{F_C'^{(1)}}^{D_{BL}} \left(\frac{1}{\lambda_{TD}^{(2c)}(y')} - 1 \right) dy' + 1 - \frac{8}{\pi^2} \sum_{n=0}^{\infty} \left[\frac{1}{(2n+1)^2} \exp\left(\frac{-(2n+1)^2 \pi^2 t_D}{4\gamma_L} \right) \right] \quad (A1)
 \end{aligned}$$

$$\begin{aligned}
 p'_{wD}(t_D) = & t_D \int_0^{D_\beta} \left(\frac{1}{\lambda_{TD}^{(2a)}(y')} - 1 \right) dy' + t_D \left(\frac{1}{\lambda_{TD}^{(2b)}} - 1 \right) (F_C'^{(1)} - D_\beta) \\
 & + t_D \int_{F_C'^{(1)}}^{D_{BL}} \left(\frac{1}{\lambda_{TD}^{(2c)}(y')} - 1 \right) dy' + \frac{2t_D}{\gamma_L} \sum_{n=0}^{\infty} \left[\exp\left(\frac{-(2n+1)^2 \pi^2 t_D}{4\gamma_L} \right) \right]. \quad (A2)
 \end{aligned}$$

Appendix A.2. Before Zone 2b Breaks Through: $\frac{1}{D_{BL}} < t_D < \frac{1}{F'_C(1)}$

$$p_{wD}(t_D) = t_D \int_0^{D_\beta} \left(\frac{1}{\lambda_{TD}^{(2a)}(y')} - 1 \right) dy' + t_D \left(\frac{1}{\lambda_{TD}^{(2b)}} - 1 \right) (F'_C(1) - D_\beta) + t_D \int_{F'_C(1)}^{\frac{1}{t_D}} \left(\frac{1}{\lambda_{TD}^{(2c)}(y')} - 1 \right) dy' + 1 - \frac{8}{\pi^2} \sum_{n=0}^{\infty} \left[\frac{1}{(2n+1)^2} \exp\left(\frac{-(2n+1)^2 \pi^2 t_D}{4\gamma_L} \right) \right] \quad (A3)$$

$$p'_{wD}(t_D) = t_D \int_0^{D_\beta} \left(\frac{1}{\lambda_{TD}^{(2a)}(y')} - 1 \right) dy' + t_D \left(\frac{1}{\lambda_{TD}^{(2b)}} - 1 \right) (F'_C(1) - D_\beta) + t_D \int_{F'_C(1)}^{\frac{1}{t_D}} \left(\frac{1}{\lambda_{TD}^{(2c)}(y')} - 1 \right) dy' - \left(\frac{1}{\lambda_{TD}^{(2c)}(y' = \frac{1}{t_D})} - 1 \right) + \frac{2t_D}{\gamma_L} \sum_{n=0}^{\infty} \left[\exp\left(\frac{-(2n+1)^2 \pi^2 t_D}{4\gamma_L} \right) \right]. \quad (A4)$$

The variable $\lambda_{TD}^{(2c)}(y' = \frac{1}{t_D})$ denotes the total mobility at the outlet at time t_D .

Appendix A.3. Before Zone 2a Breaks Through: $\frac{1}{F'_C(1)} < t_D < \frac{1}{D_\beta}$

$$p_{wD}(t_D) = t_D \int_0^{D_\beta} \left(\frac{1}{\lambda_{TD}^{(2a)}(y')} - 1 \right) dy' + t_D \left(\frac{1}{\lambda_{TD}^{(2b)}} - 1 \right) \left(\frac{1}{t_D} - D_\beta \right) + 1 - \frac{8}{\pi^2} \sum_{n=0}^{\infty} \left[\frac{1}{(2n+1)^2} \exp\left(\frac{-(2n+1)^2 \pi^2 t_D}{4\gamma_L} \right) \right] \quad (A5)$$

$$p'_{wD}(t_D) = t_D \int_0^{D_\beta} \left(\frac{1}{\lambda_{TD}^{(2a)}(y')} - 1 \right) dy' - t_D D_\beta \left(\frac{1}{\lambda_{TD}^{(2b)}} - 1 \right) + \frac{2t_D}{\gamma_L} \sum_{n=0}^{\infty} \left[\exp\left(\frac{-(2n+1)^2 \pi^2 t_D}{4\gamma_L} \right) \right] \quad (A6)$$

Appendix A.4. After Zone 2a Breaks Through: $t_D > \frac{1}{D_\beta}$

$$p_{wD}(t_D) = t_D \int_0^{\frac{1}{t_D}} \left(\frac{1}{\lambda_{TD}^{(2a)}(y')} - 1 \right) dy' + 1 - \frac{8}{\pi^2} \sum_{n=0}^{\infty} \left[\frac{1}{(2n+1)^2} \exp\left(\frac{-(2n+1)^2 \pi^2 t_D}{4\gamma_L} \right) \right] \quad (A7)$$

$$p'_{wD}(t_D) = t_D \int_0^{\frac{1}{t_D}} \left(\frac{1}{\lambda_{TD}^{(2a)}(y')} - 1 \right) dy' - \left(\frac{1}{\lambda_{TD}^{(2a)}\left(y' = \frac{1}{t_D}\right)} - 1 \right) + \frac{2t_D}{\gamma_L} \sum_{n=0}^{\infty} \left[\exp\left(\frac{-(2n+1)^2 \pi^2 t_D}{4\gamma_L} \right) \right]. \quad (A8)$$

References

1. Lake, L.W. *Enhanced Oil Recovery*; Prentice-Hall: Englewood Cliffs, NJ, USA, 1989.
2. Koottungal, L. Worldwide EOR Survey. *Oil Gas J.* **2014**, *112*, 79–91.
3. Bray, R.C. Gas Injection and Miscible Flooding. In Proceedings of the 8th World Petroleum Congress, Moscow, Russia, 13–19 June 1971.
4. Orr, F.M., Jr. *Theory of Gas Injection Processes*; Tie-Line Publications: Copenhagen, Denmark, 2007.
5. Johnson, E.F.; Welge, H.J. An Analysis of the Linear Displacement of Oil by Gas-Driven Solvent. In Proceedings of the Fall Meeting of the Society of Petroleum Engineers of AIME, Dallas, TX, USA, 21 September–1 October 1957.
6. Welge, H.; Johnson, E.; Ewing, S.; Brinkman, F. The Linear Displacement of Oil from Porous Media by Enriched Gas. *J. Pet. Technol.* **1961**, *13*, 787–796. [[CrossRef](#)]
7. Buckley, S.E.; Leverett, M.C. Mechanism of Fluid Displacement in Sands. *Trans. AIME* **1942**, *146*, 107–116. [[CrossRef](#)]
8. Wachmann, C. A Mathematical Theory for the Displacement of Oil and Water by Alcohol. *SPE J.* **1964**, *04*, 250–266. [[CrossRef](#)]
9. Larson, R.G. The Influence of Phase Behavior on Surfactant Flooding. *SPE J.* **1979**, *19*, 411–422. [[CrossRef](#)]
10. Hirasaki, G.J. Application of the Theory of Multicomponent, Multiphase Displacement to Three-Component, Two-Phase Surfactant Flooding. *SPE J.* **1981**, *21*, 191–204. [[CrossRef](#)]
11. Hirasaki, G.J. Ion Exchange with Clays in the Presence of Surfactant. *SPE J.* **1982**, *22*, 181–192. [[CrossRef](#)]
12. Dumore, J.M.; Hagoort, J.; Risseuw, A.S. An Analytical Model for One-Dimensional, Three-Component Condensing and Vaporizing Gas Drives. *SPE J.* **1984**, *24*, 169–179. [[CrossRef](#)]
13. Helfferich, F.G. Theory of Multicomponent, Multiphase Displacement in Porous Media. *SPE J.* **1981**, *21*, 51–62. [[CrossRef](#)]
14. Monroe, W.W.; Silva, M.K.; Larson, L.L.; Orr, F.M., Jr. Composition Paths in Four-Component Systems: Effect of Dissolved Methane on 1D CO₂ Flood Performance. *SPE Reserv. Eng.* **1990**, *5*, 423–432. [[CrossRef](#)]
15. Dindoruk, B.; Johns, R.T.; Orr, F.M., Jr. Analytical Solution for Four Component Gas Displacements with Volume Change on Mixing. In Proceedings of the 3rd European Conference on the Mathematics of Oil Recovery, Delft, The Netherlands, 17–19 June 1992.
16. Johns, R.T. Analytical Theory of Multicomponent Gas Drives with Two-Phase Mass Transfer. Ph.D. Thesis, Stanford University, Palo Alto, FL, USA, 1992.
17. Seto, C.J.; Jessen, K.; Orr, F.M., Jr. A Multicomponent, Two-Phase-Flow Model for CO₂ Storage and Enhanced Coalbed-Methane Recovery. *SPE J.* **2009**, *14*, 30–40. [[CrossRef](#)]
18. Johns, R.T.; Orr, F.M., Jr. Miscible Gas Displacement of Multicomponent Oils. *SPE J.* **1996**, *01*, 39–50. [[CrossRef](#)]
19. Pires, A.P.; Bedrikovetsky, P.G.; Shapiro, A.A. Analytical Model for 1-D Gas Flooding: Splitting Between Hydrodynamics and Thermodynamics. In Proceedings of the SPE/DOE Improved Oil Recovery Symposium, Tulsa, OK, USA, 22–26 April 2004.
20. Zhu, J.; Jessen, K.; Orr, F.M., Jr. Analytical Solution for Gas/Oil Displacement with Temperature Variation. In Proceedings of the SPE/DOE Improved Oil Recovery Symposium, Tulsa, OK, USA, 17–21 April 2004.
21. LaForce, T.C.; Johns, R.T. Composition Routes for Three-Phase Partially Miscible Flow in Ternary Systems. *SPE J.* **2005**, *10*, 161–174. [[CrossRef](#)]
22. Barros, W.Q.; Pires, A.P.; Peres, A.M. Analytical solution for one-dimensional three-phase incompressible flow in porous media for concave relative permeability curves. *Int. J. Non-Linear Mech.* **2021**, *137*, 103792. [[CrossRef](#)]
23. Abbaszadeh, M.; Kamal, M. Pressure-Transient Testing of Water-Injection Wells. *SPE Reserv. Eng.* **1989**, *4*, 115–124. [[CrossRef](#)]
24. Bratvold, R.B.; Horne, R.N. Analysis of Pressure-Falloff Tests Following Cold-Water Injection. *SPE Form. Eval.* **1990**, *05*, 293–302. [[CrossRef](#)]
25. Thompson, L.G.; Reynolds, A.C. Well Testing for Radially Heterogeneous Reservoirs under Single and Multiphase Flow Conditions. *SPE Form. Eval.* **1997**, *12*, 57–64. [[CrossRef](#)]
26. Peres, A.; Reynolds, A. Theory and Analysis of Injectivity Tests on Horizontal Wells. *SPE J.* **2003**, *08*, 147–159. [[CrossRef](#)]
27. Boughrara, A.A.; Peres, A.M.; Chen, S.; Machado, A.A.V.; Reynolds, A.C. Approximate Analytical Solutions for the Pressure Response at a Water-Injection Well. *SPE J.* **2007**, *12*, 19–34. [[CrossRef](#)]
28. Habte, A.D.; Onur, M.; Saaid, I.B.M.; Ofei, T.N. Pressure-Transient Behavior of Injection/Falloff Tests. In *International Conference on Integrated Petroleum Engineering and Geosciences*; Springer Publishing: Kuala Lumpur, Malaysia, 2017; pp. 83–96.

29. Machado, C.G.; Firoozabad, M.M.; Reynolds, A.C. Carbon Dioxide Effects on Wellbore-Pressure Response During Injection/Falloff Test. *SPE J.* **2018**, *23*, 919–936. [[CrossRef](#)]
30. Mu, L.; Liao, X.; Chen, Z.; Zou, J.; Chu, H.; Li, R. Analytical Solution of Buckley-Leverett Equation for Gas Flooding Including the Effect of Miscibility with Constant-Pressure Boundary. *Energy Explor. Exploit.* **2019**, *37*, 960–991. [[CrossRef](#)]
31. Cantagesso, L.C.M.; Sousa, L.K.S.; Marotto, T.A.; Radovanovic, A.M.; Pires, A.P.; Peres, A.M.M. A Semi-Analytical Solution for One-dimensional Oil Displacement by Miscible Gas in a Homogeneous Porous Media. In Proceedings of the International Conference on Integral Methods in Science and Engineering, Brighton, UK, 16–20 July 2018.
32. Nichele, J.; Teixeira, D.A. Evaluation of Darcy–Brinkman equation for simulations of oil flows in rocks. *J. Pet. Sci. Eng.* **2015**, *134*, 76–78. [[CrossRef](#)]
33. Hustad, O.S.; Holt, T. Gravity Stable Displacement of Oil by Hydrocarbon Gas After Waterflooding. In Proceedings of the SPE/DOE Enhanced Oil Recovery Symposium, Tulsa, OK, USA, 22 April 1992. [[CrossRef](#)]
34. Dyer, S.B.; Farouq Ali, S.M. Linear Model Studies of the Immiscible CO₂ WAG Process for Heavy-Oil Recovery. *SPE Reserv. Eng.* **1994**, *9*, 107–111. [[CrossRef](#)]
35. Fatemi, S.M.; Sohrabi, M. Cyclic Hysteresis in Three-Phase Relative Permeability Applicable to WAG Injection: Water-Wet and Mixed-Wet Systems under Low Gas/Oil IFT. In Proceedings of the SPE Annual Technical Conference and Exhibition, San Antonio, TX, USA, 8–10 October 2012. [[CrossRef](#)]
36. Fatemi, S.M.; Sohrabi, M. Experimental and Theoretical Investigation of Water/Gas Relative Permeability Hysteresis: Applicable to Water Alternating Gas (WAG) Injection and Gas Storage Processes. In Proceedings of the Abu Dhabi International Petroleum Conference and Exhibition, Abu Dhabi, United Arab Emirates, 11–14 November 2012. [[CrossRef](#)]
37. Fatemi, S.M.; Sohrabi, M. Experimental Investigation of Near-Miscible Water-Alternating-Gas Injection Performance in Water-Wet and Mixed-Wet Systems. *SPE J.* **2013**, *18*, 114–123. [[CrossRef](#)]
38. Zhang, C.; Oostrom, M.; Wietsma, T.W.; Grate, J.W.; Warner, M.G. Influence of Viscous and Capillary Forces on Immiscible Fluid Displacement: Pore-Scale Experimental Study in a Water-Wet Micromodel Demonstrating Viscous and Capillary Fingering. *Energy Fuels* **2011**, *25*, 3493–3505. [[CrossRef](#)]
39. Yang, Y.; Horne, R.N.; Cai, J.; Yao, J. Recent advances on fluid flow in porous media using digital core analysis technology. *Adv. Geo-Energy Res.* **2023**, *9*, 71–75. [[CrossRef](#)]
40. Zou, S.; Chen, D.; Kang, N.; Xie, C.; Armstrong, R.T.; Cai, J. An Experimental Investigation on the Energy Signature Associated With Multiphase Flow in Porous Media Displacement Regimes. *Water Resour. Res.* **2024**, *60*, e2023WR036241. [[CrossRef](#)]
41. Irannezhad, A.; Primkulov, B.K.; Juanes, R.; Zhao, B. Fluid-fluid displacement in mixed-wet porous media. *Phys. Rev. Fluids* **2023**, *8*, L012301. [[CrossRef](#)]
42. Irannezhad, A.; Primkulov, B.K.; Juanes, R.; Zhao, B. Characteristics of fluid–fluid displacement in model mixed-wet porous media: Patterns, pressures and scalings. *J. Fluid Mech.* **2023**, *967*, A27. [[CrossRef](#)]
43. Li, J.; Cui, C.; Wu, Z.; Yi, J.; Zong, R.; Fu, Y.; Han, X. Simulation of Microscopic Seepage Characteristics of Interphase Mass Transfer in CO₂ Miscible Flooding under Multiphysics Field Coupling Conditions. *ACS Omega* **2023**, *8*, 10062–10076. [[CrossRef](#)] [[PubMed](#)]
44. Christensen, J.; Stenby, E.; Skauge, A. Compositional and Relative Permeability Hysteresis Effects on Near-Miscible WAG. In Proceedings of the SPE/DOE Improved Oil Recovery Symposium, Tulsa, OK, USA, 19–22 April 1998. [[CrossRef](#)]
45. Li, D.; Kumar, K.; Mohanty, K.K. Compositional Simulation of WAG Processes for a Viscous Oil. In Proceedings of the SPE Annual Technical Conference and Exhibition, Denver, CO, USA, 5–8 October 2003. [[CrossRef](#)]
46. Chen, X.; Yu, H.; Cao, A.; Yang, Z.; Li, W.; Niu, Z.; Chang, Y.; Du, M. Study on Enhanced Oil Recovery Mechanism of CO₂ Miscible Flooding in Heterogeneous Reservoirs under Different Injection Methods. *ACS Omega* **2023**, *8*, 24663–24672. [[CrossRef](#)] [[PubMed](#)]
47. Ren, J.; Xiao, W.; Pu, W.; Tang, Y.; Bernabé, Y.; Cheng, Q.; Zheng, L. Characterization of CO₂ miscible/immiscible flooding in low-permeability sandstones using NMR and the VOF simulation method. *Energy* **2024**, *297*, 131211. [[CrossRef](#)]
48. Zhu, Q.; Wu, K.; Guo, S.; Peng, F.; Zhang, S.; Jiang, L.; Li, J.; Feng, D.; Zhang, Y.; Chen, Z. Pore-scale investigation of CO₂-oil miscible flooding in tight reservoir. *Appl. Energy* **2024**, *368*, 123439. [[CrossRef](#)]
49. Pires, A.P.; Bedrikovetsky, P.G. Analytical Modeling of 1D n-Component Miscible Displacement of Ideal Fluids. In Proceedings of the SPE Latin American and Caribbean Petroleum Engineering Conference, Rio de Janeiro, Brazil, 20–23 June 2005.
50. Peng, D.Y.; Robinson, D.B. A New Two-Constant Equation of State. *Ind. Eng. Chem. Fundam.* **1976**, *15*, 59–64. [[CrossRef](#)]
51. Corey, A.T. The Interrelation Between Gas and Oil Relative Permeabilities. *Prod. Mon.* **1954**, *19*, 38–41.

52. Bedrikovetsky, P. *Mathematical Theory of Oil and Gas Recovery*; Springer: Dordrecht, The Netherlands, 1993.
53. Bourdet, D.; Whittle, T.M.; Douglas, A.A.; Pirard, Y.M. A New Set of Type Curves Simplifies Well Test Analysis. *World Oil* **1983**, *196*, 95–106.

Disclaimer/Publisher’s Note: The statements, opinions and data contained in all publications are solely those of the individual author(s) and contributor(s) and not of MDPI and/or the editor(s). MDPI and/or the editor(s) disclaim responsibility for any injury to people or property resulting from any ideas, methods, instructions or products referred to in the content.